Chemical Geology 587 (2022) 120613

Contents lists available at ScienceDirect

Chemical Geology

journal homepage: www.elsevier.com/locate/chemgeo

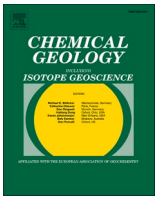

Effect of barite-bound Sr on detrital Sr isotope systematics in marine sediments

Jiawang Wu [a,b,f,*], Zhifei Liu [a], Annie Michard [c], Kazuyo Tachikawa [c], Amalia Filippidi [b], Zhiwei He [a], Rick Hennekam [b,d], Shouye Yang [a], Gareth R. Davies [e], Gert J. de Lange [a,b]

[a] State Key Laboratory of Marine Geology, School of Earth and Ocean Science, Tongji University, Siping 1239, 200092 Shanghai, China
[b] Department of Earth Sciences–Geochemistry, Faculty of Geosciences, Utrecht University, Princetonplein 9, 3584 CC Utrecht, the Netherlands
[c] Aix Marseille University, CNRS, IRD, INRAE, Coll France, CEREGE, 13545 Aix-en-Provence, France
[d] Department of Ocean Systems, NIOZ Royal Netherlands Institute for Sea Research, P.O. Box 59, 1790 AB Den Burg, the Netherlands
[e] Geology & Geochemistry, Department of Earth Sciences, VU Amsterdam University, De Boelelaan 1085, 1081 HV Amsterdam, the Netherlands
[f] School of Marine Sciences, Sun Yat-Sen University, SYSU Zhuhai Campus, 519082 Guangdong, China

ARTICLE INFO

Editor: Michael E. Boettcher

Keywords:
Strontium (Sr)
Sr isotopes
Barite
Barium (Ba)
Sapropel
Mediterranean Sea
Provenance
Marine sediments

ABSTRACT

In marine sediments, the Sr content and isotope composition ($^{87}Sr/^{86}Sr$) of the terrigenous detrital component are widely used to track changes in provenance and related transport and weathering processes. Accurately separating detrital-Sr from other sedimentary Sr-phases is a prerequisite for such studies. Conventionally, it is assumed that Sr in the carbonate-free residue corresponds to detrital Sr alone. However, the decarbonated residue may contain barite with significant Sr content and a non-detrital $^{87}Sr/^{86}Sr$ composition; this may substantially affect the measured Sr signal. To examine this chronically overlooked phenomenon, the Mediterranean Sea is an ideal area because 1) detailed provenance studies have been done using Sr and $^{87}Sr/^{86}Sr$ of the residual fraction, and 2) enhanced levels of barite repeatedly occurred in association with distinct, organic-rich sapropel sediments.

Here, we use the most-recent sapropel S1 interval to evaluate the effect of barite-bound Sr in the residual fraction after decarbonation. A total of 130 samples were taken from 10 cores in the eastern Mediterranean Sea (EMS) and 1 core in the western Mediterranean Sea. This selection represents a geographic and bathymetric coverage of the EMS and permits the basin-wide comparison between organic-rich and -lean sediments. After decarbonation using 1 M HCl solution, the residual sediments were subject to NH_4Cl extraction (2 M, pH 7), known to selectively dissolve barite. Our results demonstrate the presence of Sr-bearing barite after traditional carbonate removal and its effect on the derived "detrital" Sr signature. This barite-Sr effect is considerable for samples with barite-Ba >400 μg/g in bulk sediment. The impact of barite is prominent if accompanied by a detrital provenance background of high $^{87}Sr/^{86}Sr$ (>0.713) or low Sr/Al (<1.0 mg/g). In such cases, removal of remaining barite is required to obtain an unbiased detrital Sr signal. We recommend an improved procedure for detrital Sr separation in marine sediments, with an additional NH_4Cl leaching step to eliminate any remaining barite after decarbonation. This approach is particularly important for areas/times of high biological productivity, where sediments are often characterized by abundant barite content.

1. Introduction

The strontium (Sr) concentration and isotope ratio ($^{87}Sr/^{86}Sr$) in terrigenous, fine-grained sediments accumulating on the seafloor are commonly governed by detrital minerals from two end-member sources (Dasch, 1969): 1) the weathering products of predominantly young volcanic rocks (high Sr, $^{87}Sr/^{86}Sr = 0.704 \pm 0.002$) and 2) those of old continental crust (low Sr, $^{87}Sr/^{86}Sr \geq 0.730$). As a fingerprint of source rocks, the Sr content and $^{87}Sr/^{86}Sr$ composition are widely employed to trace the provenance of silicate detritus in marine sediments (Grousset et al., 1998; Krom et al., 1999; Hemming et al., 2007; Rutberg et al., 2005; Stein et al., 2007; Box et al., 2011). Variations in $^{87}Sr/^{86}Sr$ ratios have alternatively been interpreted to reflect changes in continental hydrology, weathering regimes, and atmospheric inputs, due to the

* Corresponding author now at: School of Marine Sciences, Sun Yat-Sen University, SYSU Zhuhai Campus, 519082 Guangdong, China.
E-mail addresses: jwwu@tongji.edu.cn, wujiaw5@mail.sysu.edu.cn (J. Wu).

https://doi.org/10.1016/j.chemgeo.2021.120613
Received 4 June 2021; Received in revised form 25 October 2021; Accepted 29 October 2021
Available online 30 October 2021

contrasts in geochemical properties between radioactively decaying parent ^{87}Rb and daughter ^{87}Sr (Nesbitt et al., 1980; Blum and Erel, 1995; Jung et al., 2004; Colin et al., 2006; Vance et al., 2009). Moreover, $^{87}Sr/^{86}Sr$ ratios seem to differentiate during transport processes of mineralogically different grain-size fractions, related to transport processes (Eisenhauer et al., 1999; Walter et al., 2000; Grousset and Biscaye, 2005; Feng et al., 2009; Meyer et al., 2011). Recently, stable Sr isotopes ($\delta^{88/86}Sr$) of rivers were linked to silicate and carbonate weathering (Wei et al., 2013; Stevenson et al., 2018), and the seawater $\delta^{88/86}Sr$ record may reflect changes in both marine Sr sources and carbonate sink (Krabbenhöft et al., 2010; Pearce et al., 2015; Paytan et al., 2021). Hence, for provenance and weathering studies, the use of Sr systematics is often combined with more conservative proxies, such as Nd isotopes that are little affected by most sedimentary processes (Freydier et al., 2001; Weldeab et al., 2002; Liu et al., 2007; Cole et al., 2009; Revel et al., 2010; Xie and Marcantonio, 2012; Wu et al., 2016, 2018; Blanchet et al., 2021).

All these studies rely on the accurate separation of terrigenous detrital Sr from marine sediments. However, the potential impact of Sr in marine barite was usually ignored. In marine sediments, three main sources of Sr occur (Kastner, 1999): detrital, biogenic (including carbonate), and authigenic (including barite; termed as "hydrogenetic" here; Fantle et al., 2020). For most – if not all – studies, the routine method is to treat bulk sediments with acid, thus removing the biogenic Sr predominantly present in carbonate; the carbonate-free residue is commonly assumed to be of detrital origin only. This leaching is either done with HCl (Jung et al., 2004; Liu et al., 2007; Box et al., 2011; Meyer et al., 2011) or acetic acid (Bayon et al., 2002; Weldeab et al., 2002; Colin et al., 2006; Cole et al., 2009), both proven to be effective in removing carbonate Sr. Minor Sr may be dissolved from the aluminosilicate minerals during the leaching. The amount of Sr released depends on acid type/strength, reaction time, and mineralogy of the sample itself, but is negligible compared to the remaining detrital Sr (Lyle et al., 1984; Tribovillard et al., 1996; Bayon et al., 2002; Tachikawa et al., 2004). However, such decarbonation of marine sediments only partially removes the Sr associated with the mineral barite ($BaSO_4$).

Although seawater is largely undersaturated with respect to barite (Rushdi et al., 2000; Monnin and Cividini, 2006), barite is found throughout the ocean as microcrystals and aggregates of 0.5–5-μm-size grains (Church and Wolgemuth, 1972; Dehairs et al., 1980; Bishop, 1988; Griffith and Paytan, 2012). Marine barite is a ubiquitous minor phase in marine sediments (~0.2–2% on a $CaCO_3$-free basis), especially in those underlying areas of high biological productivity; but its exact formation mechanism is still not fully clarified (see reviews by Paytan and Griffith, 2007; Martinez-Ruiz et al., 2019). No planktonic organism has been identified to account for the abundance of barite (Bertram and Cowen, 1997), suggesting that marine barite mainly precipitates in the upper water column, where most of the organic matter is regenerated (Griffith and Paytan, 2012; Martinez-Ruiz et al., 2019; and references therein). This process is thought to occur within micro-environments in association with decaying organic matter (Dehairs et al., 1980; Bishop, 1988; Dymond et al., 1992; Ganeshram et al., 2003), and seems accompanied by microbial activity (Gonzalez-Munoz et al., 2012; Torres-Crespo et al., 2015; Martinez-Ruiz et al., 2018, 2019). Alternatively, it may relate to dissolution of acantharian Ba-rich celestite ($SrSO_4$) skeletons (Bernstein et al., 1992, 1998; Bertram and Cowen, 1997; van Beek et al., 2007),

Barite has a high affinity for incorporating Sr – being a chemical analogue of Ba – into its lattice (~0.7–3% of Sr; Averyt et al., 2003; Monnin and Cividini, 2006). A recent study has shown that organic films can promote locally favorable environments for barite formation under the competitive adsorption of Ba and Sr, and can enhance the Sr enrichment in barite during the nucleation stage (Deng et al., 2019a). This finding may explain the observation that the Sr content depends on crystalline habit and morphology of the barite (Bertram and Cowen, 1997), as Sr-enriched barite is expected to be less stable in seawater (Bishop, 1988; Rushdi et al., 2000; van Beek et al., 2003; Monnin and Cividini, 2006). Moreover, the variability of Sr content in barite may represent various stages between the initial process of barite precipitation in the water column and its transformation to the crystals found in marine sediment (Martinez-Ruiz et al., 2019).

Barite is a highly insoluble mineral, even in acids (Ksp: $\sim 10^{-10}$; Church and Wolgemuth, 1972). Previous studies have suggested that multi-step acid leaching cannot fully remove barite (Lyle et al., 1984; Paytan et al., 1993; Tribovillard et al., 1996; Eagle et al., 2003; Ziegler et al., 2007; Wu et al., 2017). In fact, barite is characterized by good preservation in oxic pelagic sediments and conservative behavior during early diagenesis (Paytan and Kastner, 1996; Van Santvoort et al., 1996; McManus et al., 1998; Schenau et al., 2001). These characteristics have made barite a useful proxy for ocean productivity (Dymond et al., 1992; Francois et al., 1995; Paytan and Griffith, 2007) and a recorder of seawater chemistry (e.g. Sr isotopes and Sr/Ba ratio; Paytan et al., 1993, 2021; Averyt and Paytan, 2003; van Beek et al., 2003).

However, the refractory nature of barite also prevents an adequate removal by conventional decarbonation, leaving the barite-bound Sr mixed with the detrital Sr in the residue. This is likely to affect the Sr isotope systematics of "detrital" component derived from the decarbonated sediment. To our knowledge, there are only two studies reporting the possible survival of barite in the acid-leached residual fraction, but this phenomenon was thought to be unique within the equatorial upwelling zones of the Pacific (i.e. $<3^{\circ}$ proximity to the equator) (Ziegler et al., 2007; Xie and Marcantonio, 2012). An examination for this chronically overlooked and potentially misleading deviation is required. In this respect, the Mediterranean Sea has an ideal setting because 1) Sr isotopes of the residual fraction have been widely used to distinguish detrital provenance (Krom et al., 1999; Weldeab et al., 2002; Wu et al., 2016; Blanchet et al., 2021), and 2) the sediments are marked by the rhythmic occurrence of organic-rich sapropel layers with enhanced barite content (Rossignol-Strick et al., 1982; Van Santvoort et al., 1996; De Lange et al., 2008; Rohling et al., 2015).

Here, we present an in-depth investigation and overview with pertinent examples for Mediterranean sediments. Relying on the organic- and barite-rich sapropel S1 layer, a total of 130 samples from 11 Mediterranean cores are used to demonstrate the survival of barite-Sr after decarbonation, and to evaluate potential effects of barite-Sr content on detrital provenance studies (Fig. 1; Table 1). A novel scheme comprising decarbonation and barite-specific extraction is designed to remove any barite-bound Sr after carbonate removal (Fig. 2; Table 2). The set-up permits us to address 1) a comparison between sapropel samples with quantified barite content and non-sapropel samples with no/negligible barite; and 2) the basin-wide differences in terms of barite abundance and provenance signal. Subsequently, we determine the factors that cause a significant effect of barite-Sr on the detrital Sr isotope composition, and recommend an adequate leaching procedure for future studies, particularly those in high-productivity regions or time intervals.

2. Background

2.1. Mediterranean and sapropel layers

The Mediterranean is an ideal area to examine the inferred impact of barite-Sr on the use of detrital Sr systematics. The $^{87}Sr/^{86}Sr$ ratio and Sr concentration of decarbonated sediments have been widely used as provenance proxies over the circum-Mediterranean region (e.g. Krom et al., 1999; Freydier et al., 2001; Weldeab et al., 2002; Revel et al., 2010; Box et al., 2011; Scheuvens et al., 2013; Wu et al., 2016, 2018; Blanchet et al., 2021). Major terrigenous supplies from Saharan Dust, Nile River, northern-borderlands rivers, and North-African paleo-rivers have been identified (Fig. 1).

Mediterranean sediments are marked by the cyclic occurrence of organic-rich units called sapropels, concurrent with enhanced barite

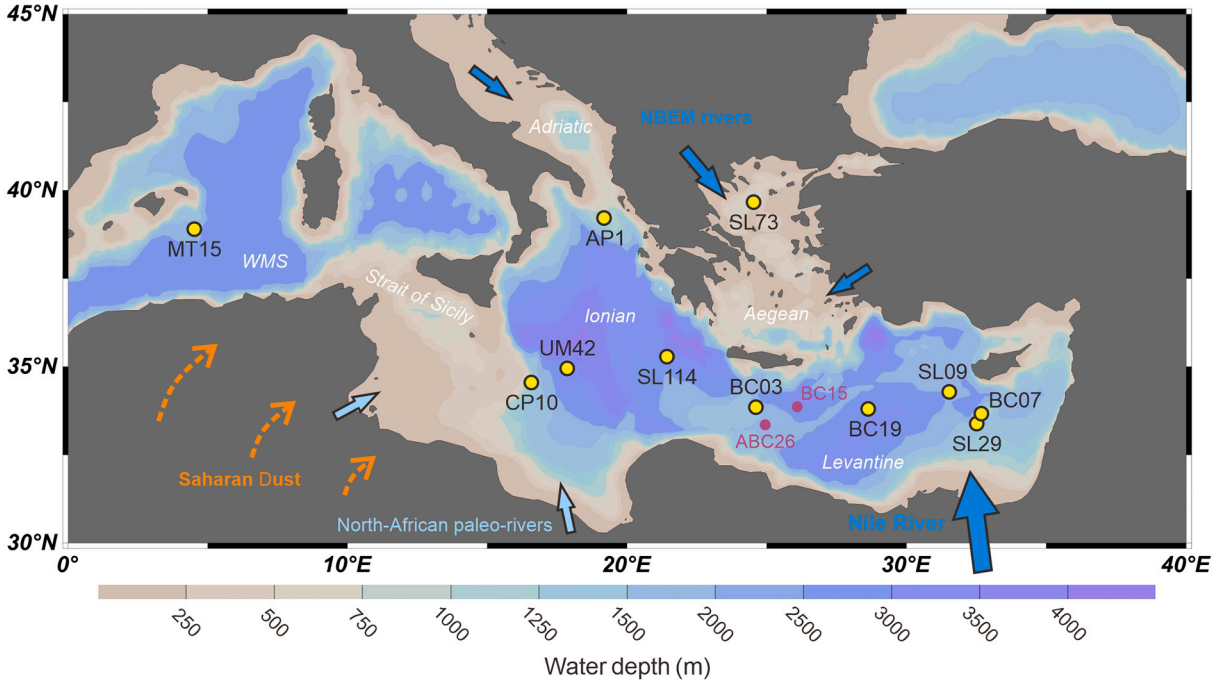

Fig. 1. Bathymetric map of the Mediterranean Sea, showing the locations of studied cores (yellow circles; Table 1) and the cores subject to detailed barite-specific method of BASEX (purple circles; Rutten and de Lange, 2002). General provenance background is depicted: Saharan Dust, Nile River, riverine inputs from the NBEM (i.e. northern borderlands of eastern Mediterranean), and the potential paleo-rivers from North Africa (cf. Wu et al., 2016, 2018).

Table 1
General information of the Mediterranean cores investigated.

Core[a]	Type[b]	Water depth	Location	Cruise	Data reference[c]
SL73	BC	339 m	39°39.7′N, 24°30.7′E	RV *Logachev* 1999	T04, D08, W18
AP1	GC	811 m	39°13.0′N, 19°06.8′E	RV *Urania* 1998	T04, D08
BC07	BC	893 m	33°40.0′N, 32°40.0′E	RV *Marion Dufresne* 1994/5	F01, W18
UM42	BC	1375 m	34°57.2′N, 17°51.8′E	RV *Urania* 1994	F01, D08
CP10	BC	1501 m	34°32.7′N, 16°34.0′E	RV *Pelagia* 2011	W16, W17
SL29	BC	1587 m	33°23.4′N, 32°30.2′E	RV *Logachev* 1999	D08
BC03	BC	2180 m	33°22.5′N, 24°46.0′E	RV *Marion Dufresne* 1994/5	F01, T04, W18
SL09	BC	2302 m	34°17.2′N, 31°31.4′E	RV *Logachev* 1999	T04, R06a, D08, W18
BC19	BC	2750 m	33°47.9′N, 28°36.5′E	RV *Marion Dufresne* 1991	F01, RL02, S02, S04, T04, R06b, D08, W18
SL114	BC	3390 m	35°17.2′N, 21°24.5′E	RV *Logachev* 1999	S04, T04, R06a, D08, W16, W19
MT15	PC	2373 m	38°53.8′N, 04°30.6′E	RV *Tyro* 1993	T04, W19

[a] All cores collected from the eastern Mediterranean Sea (EMS), except for MT15 from the western Mediterranean Sea (WMS).
[b] Types of the corer: box core (BC), gravity core (GC), and piston core (PC).
[c] Published data with established age models are assembled in this study: F01= Freydier et al. (2001), RL02= Rutten and de Lange (2002), S02= Slomp et al. (2002), S04= Slomp et al. (2004), T04= Tachikawa et al. (2004), R06a= Reitz et al. (2006a), R06b= Reitz et al. (2006b), D08= De Lange et al. (2008), W16= Wu et al. (2016), W17= Wu et al. (2017), W18= Wu et al. (2018), W19= Wu et al. (2019).

content. Sapropels occurred more frequently in the eastern Mediterranean Sea (EMS) than western Mediterranean Sea (WMS) (Rossignol-Strick et al., 1982; Zhao et al., 2012; Rohling et al., 2015). Sapropel formation has been attributed to stagnating deep-water conditions and/or enhanced biological production, induced by increased rainfall and river runoff (e.g. De Lange et al., 2008; Hennekam et al., 2015; Filippidi et al., 2016; Wu et al., 2019; Benkovitz et al., 2020).

The strong correlation between vertical fluxes of particulate barite and organic carbon (C_{org}) found in sediment traps (Dymond et al., 1992; Francois et al., 1995; Dehairs et al., 2000) has made barite a promising proxy for ocean productivity (see review by Paytan and Griffith, 2007). This is especially true for the Mediterranean because the Ba profiles do not appear diagenetically altered over the last 1.1 Ma (Langereis et al., 1997), as demonstrated for the most recent sapropel S1. Specifically, microscopic and geochemical studies have confirmed that such excess, biogenic Ba in sapropels is related to barite, superimposed on silicate-bound, detrital Ba (Thomson et al., 1995, 1999; Van Santvoort et al., 1996; Martinez-Ruiz et al., 2000; Rutten and de Lange, 2002; Reitz et al., 2004). Changes in saturation state due to sulfate reduction during sapropel S1 formation generally did not cause barite dissolution, as evidenced by porewater data and sulfur isotopes of associated pyrites (Thomson et al., 1995; Van Santvoort et al., 1996; Passier et al., 1997; Martinez-Ruiz et al., 2000; De Lange et al., 2008).

2.2. Ba- and Sr-associated mineralogy in marine sediments

In marine sediments, carbonate, barite, and aluminosilicate (detrital minerals, mostly clay minerals) are the major hosts of Ba and Sr, with minor amounts in phases such as organic matter, Fe-Mn oxides, and opal (Eagle et al., 2003). Specifically, carbonate is the main carrier of Sr, but not for Ba (Ba: <30–70 μg/g; Lea and Boyle, 1989; Gingele and Dahmke, 1994; Gonneea and Paytan, 2006). Barite is the dominant phase hosting non-detrital Ba and contains considerable amounts of Sr (Sr: 0.7–3%; Averyt et al., 2003; Monnin and Cividini, 2006). Organic matter typically contains <60–300 μg/g of Ba and negligible Sr (Gingele and Dahmke, 1994; Gonneea and Paytan, 2006). This is equivalent to <1% of the total Ba for C_{org}-rich sapropel samples. In any case, most of the Ba

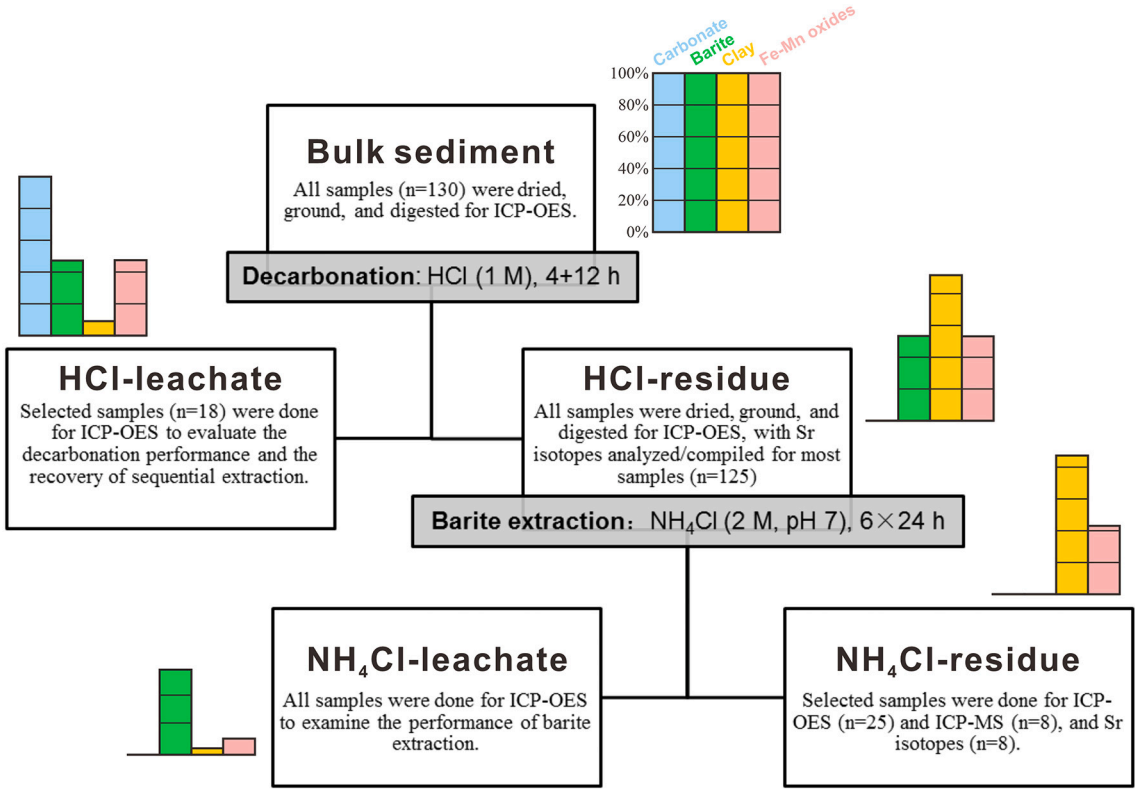

Fig. 2. Flow chart of the sequential extraction consists of decarbonation and barite extraction (Table 2). Extractions were done on Mediterranean sediments (130 samples, 11 cores), focusing on deep-sea sapropel S1 layer; and this semi-quantitative illustration is mainly after the results of CP10 as a representative core. Analytical results include Ba, Sr, Ca, Al, and Fe of different fractions (see Dataset S1). Major phases such as carbonate, barite, clay, and Fe-Mn oxides are determined for each step (see Section 3.2).

Table 2
Overview of sequential extraction procedures [a].

Step	Sample	Process	Fraction collected	Phase extracted [b]	Elements [c]	Sr isotopes [d]
1	Bulk sediments (>1 g)	Freeze-dried, ground		carbonate, barite, clay, Fe-Mn oxides	all samples (n = 130)	
2	Bulk sediments (~0.3 g)	Leached with 7.5 ml HCl (1 M) for 4 + 12 h, and rinse with 10 ml deionized water 2 times	HCl-leachate: carbonate-rich	carbonate (all), barite (part), clay (few), Fe-Mn oxides (part)	selected samples (n = 18)	
			HCl-residue: carbonate-free	barite (part), clay (most), Fe-Mn oxides (part)	all samples (n = 130)	most samples (n = 125)
3	HCl-leached residues (60–80 mg)	Leached with 6 ml NH_4Cl (2 M, pH 7) for 24 h, repeated 6 times	NH_4Cl-leachate: barite-rich	barite (most), clay (few), Fe-Mn oxides (few)	all samples (n = 130)	
			NH_4Cl-residue: carbonate- and barite-free	clay (most), Fe-Mn oxides (part)	selected samples (n = 25 + 8)	selected samples (n = 8)

[a] See also a flow chart in Fig. 2, showing the integrated results of phase separation on exemplary sapropel S1 samples of core CP10.
[b] Organic matter is disregarded due to its negligible total amounts of Ba and Sr; Fe-Mn oxides (i.e. Fe-, Mn-OOH) contain negligible Sr and only minor Ba; clay represents all detrital, aluminosilicate minerals (mostly clay minerals); see Section 3.2.
[c] Analyzed by ICP-OES (Tables S1 and S2), and a set of 8 samples by ICP-MS with replicates (Table S1).
[d] New and published data are provided for most HCl-residue samples (Table S2), with a small selection of NH_4Cl-residues analyzed for verification (Table S3).

bound to organic matter is removed during acid treatment (House and House and Norris, 2020). The Fe-Mn oxides (i.e. Fe-, Mn-OOH) contain negligible Sr and minor amounts of Ba (although sometimes considerable Ba; Van Santvoort et al., 1996; Gonneea and Paytan, 2006; Reitz et al., 2006a). There is no opal reported for our investigated sediments including sapropel S1 layers (De Lange et al., 2008; Rohling et al., 2015).

2.3. Barite determination and extraction

Determining barite content in marine sediments is important but not straightforward. Various methods have been developed. The prevalent method is to normatively calculate the excess, non-detrital Ba, i.e. total Ba in bulk sediment minus the detrital Ba estimated using an empirical Ba/Al ratio for the terrigenous, aluminosilicate component (Dymond et al., 1992; Klump et al., 2000; Eagle et al., 2003; Reitz et al., 2004). Such normative calculation, however, may introduce major errors, especially for sedimentary environments that receive large quantities of terrigenous input and/or have large variability in the Ba/Al ratio of the detrital material (Dehairs et al., 1980; Gingele and Dahmke, 1994; Fagel et al., 1999; Klump et al., 2000; Reitz et al., 2004). Besides, the calculated excess Ba may somewhat overestimate the barite content, due to the inclusion of Ba from phases other than barite and aluminosilicate, such as carbonate, organic matter, and Fe-Mn oxides (Eagle et al., 2003).

Attempts were made to directly analyze marine barite, such as by X-

ray diffraction, microscopic counting, and microprobe techniques (Dehairs et al., 1980; Gingele and Dahmke, 1994; Martinez-Ruiz et al., 2000; Robin et al., 2003; Light and Norris, 2021). However, these approaches are labor intensive and could be quantitative only for samples with barite contents exceeding 0.4% (Gingele and Dahmke, 1994; Robin et al., 2003).

A five-step sequential procedure has been widely used to isolate barite for reconstructing changes in ocean chemistry and productivity (Paytan et al., 1993, 2021; Eagle et al., 2003; Gonneea and Paytan, 2006). However, this method essentially dissolves all phases except barite, thus requires a large sample amount (~10 g), and is likely subject to partial dissolution and/or mechanical loss of barite (Fagel et al., 1999; Eagle et al., 2003; Bridgestock et al., 2019; House and Norris, 2020). Heavy liquid was also applied for barite separation (e.g. van Beek et al., 2003), but those samples are likely to contain impurities, i.e. minerals that are similarly dense and refractory as barite (e.g. anatase, rutile, monazite).

Solution analyses may be an attractive alternative. Yet, dissolving barite is not straightforward, because of its low solubility product (Ksp: $\sim 10^{-10}$, at 25 °C, 1 atm.; Church and Wolgemuth, 1972). Barite can be dissolved via resin exchange, or refluxed with sodium carbonate or lithium borate, but these methodologies usually have incomplete recovery and a significant blank (cf. Averyt et al., 2003). The ability of chelating ligands to bind Ba is documented (Lea and Boyle, 1993; Bao, 2006; Putnis et al., 2008), and a method using ligand-mediated dissolution has been reported (Xie and Marcantonio, 2012; House and Norris, 2020). This method is practical in general, but seems susceptible to various matrix effects.

A barite-specific extraction method so-called BASEX was developed for marine sediments (Schenau et al., 2001; Rutten and de Lange, 2002). This method commences with the selective extraction of barite, instead of various acid steps during which premature dissolution of barite would occur. The BASEX method is advantageous as it truly separates barite from detrital Ba-phases in the sediment (99.4% recovery of barite; Rutten and de Lange, 2002). Notably, it does not suffer from apparent matrix effects for Fe- and Mn-enriched samples as in other solution analyses (e.g. House and Norris, 2020). Modified versions of BASEX have been widely applied to determine the different particulate Ba phases, such as in the Arabian Sea and Mediterranean Sea, and for oceans like the Atlantic and Pacific (Schenau et al., 2001; Rutten and de Lange, 2002; Reitz et al., 2004, 2006a).

3. Samples, extractions, and analyses

3.1. Cores and chronologies

This study was performed on the most-recent, Holocene sapropel S1 sediments that are characterized by elevated C_{org} and Ba contents, together with the alternating intervals with organic- and Ba-lean sediment. The samples were taken from 10 basin-wide cores for the eastern Mediterranean Sea (EMS), and from one core for the western Mediterranean Sea (WMS). Note that the WMS Holocene sediments do not contain sapropel S1, but samples from the same time-interval were used. This permits a comparison between sapropel and non-sapropel contemporaneous sediments deposited in the EMS and WMS. Collectively, 130 samples from 11 cores have been studied with a geographic and bathymetric coverage of the Mediterranean Sea (Fig. 1; Table 1).

Age models were established based on radiocarbon dates, and the well-established boundaries of sapropel S1 (~9.8–5.7 ^{14}C ka; De Lange et al., 2008) as defined by the C_{org}, Ba/Al, and Mn/Al criteria (Van Santvoort et al., 1996; Thomson et al., 1999; Reitz et al., 2006a). For details of the studied cores see Table 1. Note that sapropel S1 is the only sapropel within the range of precise radiocarbon dating, allowing its depth- and process-related compositional variations to be determined through time. Sub-intervals S1a and S1b are separated by the widespread climate cooling event around 8.2 cal. ka BP (Rohling and Palike, 2005).

To avoid the complications encountered in previous radiocarbon investigations in the Mediterranean related to reservoir age and local/regional reservoir offset (ΔR) (cf. Siani et al., 2001), and also to maintain the comparability with other published records using various calibration curves (De Lange et al., 2008), the uncorrected ^{14}C ages are used here. In general, ^{14}C dates were determined on planktonic foraminifera sampled from and around the elevated zones of bulk Ba/Al; then the core-depths were converted to ^{14}C time from the regression of these radiocarbon ages versus depth (cf. De Lange et al., 2008).

3.2. Scheme of extraction procedures

A novel scheme of extraction procedures consisting of decarbonation and subsequent selective extraction of barite was used for this study (Fig. 2; Table 2). The first step is the removal of carbonate – the dominant phase of Sr – prior to selectively dissolving barite. Bulk sediment samples were leached with HCl (1 M) to remove carbonate (i.e. decarbonation), and the residues were treated with NH_4Cl (2 M, pH 7) to dissolve mainly barite (i.e. barite extraction). It was shown that the high ionic strength of NH_4Cl solvent can effectively increase barite solubility (Rutten and de Lange, 2002). This barite-specific technique is derived and simplified from the BASEX method, which has been validated using pure barite, home-made mixed mineral standard, and various marine sediments including northwest Indian Ocean upwelling sediments and Mediterranean sapropels (Schenau et al., 2001; Rutten and de Lange, 2002; Reitz et al., 2004; see also Section 2.3). Compared to the detailed BASEX extraction, our barite dissolution step is favored for its simplicity.

In our scheme, all procedures were conducted gravimetrically. For each step, the leachates including rinsing fluids were carefully collected and weighed; and the residues were dried, precisely weighed, and powdered for analyses. This permits the concentration data of all solids and fluids (including bulk sediment, and various leachates and residues) to be converted to the same basis of initial bulk sample, as reported in this contribution. An overview of the sequential extraction procedures is compiled in Table 2, with the isolated fractions and potential phases specified.

3.2.1. HCl leaching (decarbonation)

Following the protocol by Van Santvoort et al. (1996), ~0.3 g of freeze-dried, powdered bulk sediments were decarbonated by initially shaking in 7.5 ml of 1 M HCl for 4 h, and then for another 12 h after centrifuging and replacing the acids. This ensures a full removal of carbonate. Subsequently, the samples were rinsed and centrifuged twice with 10 ml deionized water, oven-dried at 80 °C and weighed.

3.2.2. NH_4Cl leaching (barite extraction)

Approximately 60–80 mg decarbonated sediment (i.e. HCl-residues) was weighed for barite extraction (Rutten and de Lange, 2002). The extraction was performed using 6 ml of NH_4Cl (2 M, pH 7) solution for 24 h. This step was repeated 6 times to have a complete dissolution of barite. The last leachates were randomly checked to confirm that no Ba and Sr had dissolved. Subsequently, the barite-free residues were rinsed with 10 ml deionized water and dried.

3.2.3. Total digestion

A routine three-step total digestion was applied for solid samples before and after all extractions (Reitz et al., 2006a; Wu et al., 2016). Powdered samples were digested in a mixture of 2.5 ml concentrated HF and 2.5 ml pre-mixed acid (3:2 concentrated $HClO_4$ and HNO_3) and heated at 90 °C in a gastight Teflon vessel for >12 h (Step-I). Subsequently, the solution was evaporated at 160 °C to near dryness (Step-II), and then the residue was dissolved in 4.5% HNO_3 at 90 °C for 6 h (Step-III). For the samples with extremely high Mn contents, the protocol was modified to a smaller aliquot of ~30 mg, with additional peroxide step to prevent Mn-oxides forming (Wu et al., 2016). This extra step involved

evaporating the sample at 160 °C with 2.5 ml concentrated H_2O_2 and 2.5 ml concentrated HCl, after the Step-II.

3.3. Geochemical measurements

3.3.1. Elemental analyses

The elemental composition was determined by Inductively Coupled Plasma – Optical Emission Spectroscopy (ICP-OES) on a Perkin-Elmer Optima 3000 or a Spectro Arcos at Utrecht. The calibration programs were designed for fluid samples or total-digested sediment samples. The ICP-OES measurements on bulk sediments were performed at different times with slightly different procedures between the cores (Slomp et al., 2002, 2004; Reitz et al., 2006a, 2006b; De Lange et al., 2008; Wu et al., 2016) (Table 1), whereas all HCl- and NH_4Cl-residues were analyzed using the same procedures. The data quality was monitored by blanks, duplicates, and international standards (ISE-921: Van Dijk and Houba, 2000; MAG-1: Govindaraju, 1994), showing the relative deviations <6% for the reported elements (i.e. Ba, Sr, Ca, Al, Fe; see Dataset S1), unless otherwise noted in Tables S1 and S2. Note that soil reference material ISE-921 having similar C_{org} contents as sapropel sediments was used to monitor systematic biases in all the extraction-related procedures.

3.3.2. Sr isotope analyses

For most samples of the decarbonated sediments, new and published Sr isotope data are provided (Freydier et al., 2001; Tachikawa et al., 2004; Wu et al., 2016) (Table S2). A total of 45 Sr isotope ratios determined by Thermal Ionization Mass Spectrometers (TIMS) are reported here, which were conducted at CEREGE ($n = 39$) and VU Amsterdam ($n = 6$) with a Finnigan MAT 262 and a Triton Plus, respectively (Table S2). After decarbonation, the samples were routinely digested in acid mixtures of HF–$HClO_4$–HNO_3; and Sr was separated from sample matrices using standard exchange techniques. The measured $^{87}Sr/^{86}Sr$ ratios were normalized to the certified NBS-SRM 987 value of 0.710248 (Thirlwall, 1991). The data uncertainties were checked by replicate analyses of NBS-SRM 987, showing external reproducibility of 0.000015 for CEREGE data (2σ SD, $n = 18$), and of 0.000016 for VU data (2σ SD, $n = 11$). Detailed analytical procedures have been described previously (CEREGE data: Freydier et al., 2001; Tachikawa et al., 2004; VU data: Meyer et al., 2011; Wu et al., 2018).

For the HCl- and NH_4Cl-leached sediments, a set of 8 samples were analyzed for Sr concentration and isotopes at Tongji University. The digestion was done with HF–HNO_3 acid mixture in high-pressure Teflon bombs, at 190 °C for >48 h (Deng et al., 2019b). An Agilent 7900 was employed to perform the Inductively Coupled Plasma – Mass Spectrometry (ICP-MS) analyses, giving the precision of <5% and accuracy of <8% for both Ba and Sr (Table S1). After standard Sr-Spec column chromatography, Sr isotope ratios were determined on a Neptune Plus Multi-Collector ICP-MS (MC-ICP-MS) (Table S3). The isotopic results were corrected for mass fractionation by normalizing to $^{86}Sr/^{88}Sr = 0.1194$. The quality of $^{87}Sr/^{86}Sr$ ratios was monitored by the standards of NBS-SRM 987, showing the mean value of 0.710235 ± 0.000021 (2σ SD, $n = 9$) within error of the recommended value of 0.710245 (Thirlwall, 1991). International reference materials BHVO-2 and AGV-2 give mean $^{87}Sr/^{86}Sr$ values of 0.703466 ± 0.000022 (2σ, $n = 2$) and of 0.703964 ± 0.000027 (2σ, n = 3), respectively. These values are within errors with the recommended values of 0.703478 ± 0.000033 and 0.703992 ± 0.000034, respectively (Jochum et al., 2005). Total procedural blanks as well as Rb and Ba levels in the measured Sr solutions were negligible (Sr <120 pg) in all cases.

4. Results and data processing

We firstly evaluate the sequential extraction procedures and the data validity (Section 4.1). As most extractions do not leach a single phase alone, multi-element analyses were performed on all leachates and residues for selected samples, to provide a complete sequential extraction for different Ba and Sr fractions (Fig. 2; Table 2). By doing so, we can check the recovery and performance of each step, and monitor the uncertainties of the data compilation and associated corrections (Fig. 3; Tables S1 and S2).

Subsequently, we demonstrate that barite was completely removed during NH_4Cl-leaching, but not fully removed during the preceding HCl decarbonation (Section 4.2). This is evident from the comparison of Ba and Sr between HCl-residues and NH_4Cl-residues (Fig. 4), and data of NH_4Cl-leachates (Fig. 5). Based on a barite Sr/Ba signature derived for deep-sea Mediterranean sediments (Fig. 6), various Ba and Sr phases are estimated and their profiles over the S1-period are displayed in Figs. 7 and 8, respectively. The leaching results of the Mediterranean sediments are compiled in Table S2.

Lastly, we correct for remaining barite-bound Sr in decarbonated sediments to evaluate the associated impact (Section 4.3). The correction of detrital Sr isotope ratios including original, corrected, and measured data (Tables S2 and S3) is shown in Fig. 9. Taken together, these results permit the effect of barite-Sr to be thoroughly examined, taking the Mediterranean as an illustration (Fig. 10).

Three groups can be distinguished between the studied Mediterranean cores, based on their barite content during the sapropel S1 period.

Group A): MT15, SL73, AP1, and BC07; S1 core samples with bulk barite-Ba content of <100–400 μg/g, corresponding to EMS cores with <1000 m water depth.

Group B): SL29, UM42, and CP10; S1 core samples with bulk barite-Ba content of ~200–800 μg/g, corresponding to EMS cores with 1000–1800 m water depth.

Group C): SL09, BC03, SL114, and BC19; S1 core samples with bulk barite-Ba content of ~300–1200 μg/g, corresponding to EMS cores with >1800 m water depth.

In general, the grouping is consistent with the depositional redox conditions: suboxic (Group A), anoxic (Group B), and euxinic (Group C) (cf. De Lange et al., 2008).

A summary of all relevant data including fractions and phases distinguished between the Groups A, B, and C is available in Supporting Information (Tables S1–S3; Figs. S1–S3; Dataset S1). Deviations in Sr isotope systematics between previously reported data on decarbonated sediments and our corrected results for barite-Sr are also shown (Figs. S4 and S5).

4.1. Evaluation of sequential extraction procedures

In our scheme, the collected fractions and residual phases containing Ba and Sr are compiled in Table 2. The fractions include initial bulk sediment, HCl-leachate, HCl-residue, NH_4Cl-leachate, and NH_4Cl-residue. In terms of Ba and Sr mass balance, the potentially significant phases comprise carbonate, barite, clay minerals, and Fe-Mn oxides, while other Ba and Sr bearing minor phases of Ba and Sr are negligible (Lea and Boyle, 1989; Gingele and Dahmke, 1994; Eagle et al., 2003; Gonneea and Paytan, 2006; House and House and Norris, 2020; see also Section 2.2). Taking the C_{org}-rich, barite-rich sapropel samples as an example, the consequent phase separation is semi-quantitatively illustrated with a flow chart of the analytical processes (Fig. 2).

Accordingly (see also Sections 2.2 and 3.2), sedimentary Ba (bulk-Ba) consists of two major components: 1) detrital, silicate-bound Ba (det-Ba) and 2) hydrogenetic, barite-related Ba (barite-Ba). Sedimentary Sr (bulk-Sr) consists of three major components: 1) carbonate-related Sr (carb-Sr), 2) detrital, silicate-bound Sr (det-Sr), and 3) hydrogenetic, barite-bound Sr (barite-Sr). These denotations are used throughout the paper.

Direct geochemical analyses were performed on selected samples of HCl-leachate and NH_4Cl-residue to monitor the recoveries for each step of the sequential extraction, as compared to the independently determined total, bulk-sediment content (Fig. 2; Table 2). For the two major steps, taking core CP10 as a representative, the HCl-leaching yields a recovery of 99% ± 4% for Ba and of 98% ± 3% for Sr (1σ, n = 18); the

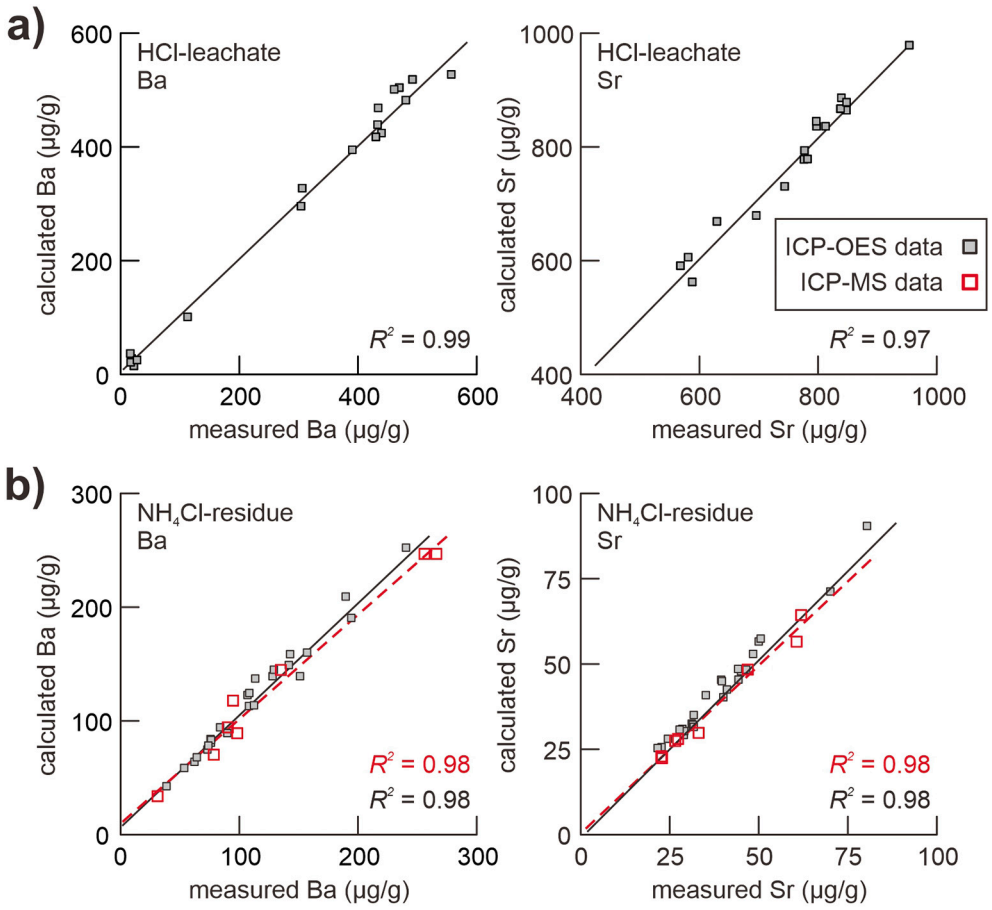

Fig. 3. Correlations between measured and calculated data in terms of Ba and Sr concentrations, on the fractions of a) HCl-leachate and b) NH_4Cl-residue, respectively (Table S1). See calculations in Section 4.1. Notably, the two sets of NH_4Cl-residue samples processed by different total-digestion and measurement methods (i.e. ICP-OES vs. ICP-MS) yield highly consistent results (Table S1). The strong correlations on selected samples justify the calculations and thus the validity for the whole dataset (Table S2).

NH_4Cl-leaching gives a recovery of 97% ± 6% for Ba and of 95% ± 6% for Sr (1σ, $n = 33$). Overall, our approach has a Ba recovery of 96–103% and a Sr recovery of 95–101% (Table S1).

Such good recoveries permit the following calculations to be made. For the fractions of HCl-leachates and NH_4Cl-residues, the Ba and Sr concentrations are calculated from the differences between bulk sediments and HCl-residues using Eq. (1), and from the differences between HCl-residues and NH_4Cl-leachates using Eq. (2), respectively (Table S2). The validity of such calculation is supported by the strong correlations ($R^2 \geq 0.97$) with the measured data of Ba and Sr, as shown for HCl-leachates (Fig. 3a) and NH_4Cl-residues (Fig. 3b).

$$Ba_{HCl-leachate} = Ba_{Bulk-sediment} - Ba_{HCl-residue} \quad (1a)$$

$$Sr_{HCl-leachate} = Sr_{Bulk-sediment} - Sr_{HCl-residue} \quad (1b)$$

$$Ba_{NH4Cl-residue} = Ba_{HCl-residue} - Ba_{NH4Cl-leachate} \quad (2a)$$

$$Sr_{NH4Cl-residue} = Sr_{HCl-residue} - Sr_{NH4Cl-leachate} \quad (2b)$$

Notably, all the concentration data reported here are relative to the same basis of initial bulk sample, allowing the mass equation expressions to be made (i.e. Eqs. (1)–(8)). For maintaining direct comparisons with published data, the mass-based unit is used here (e.g. $(Sr/Ba)_{barite}$), unless otherwise noted (i.e. the necessary use of mole-based unit: $[Sr/Ba]_{barite}$).

As described above, the good recoveries of Ba and Sr, and the strong correlation between calculated and measured data permit us to evaluate the overall leaching performance of decarbonation and barite extraction.

4.1.1. Decarbonation

It has been demonstrated that our decarbonation procedure ensures the full removal of carbonate (Van Santvoort et al., 1996; Wu et al., 2017). This is clearly seen from the tight correspondence 1) between the measured and calculated $CaCO_3$ contents (Dataset S1), and 2) between the bulk-Sr and carb-Sr profiles for all studied cores (Fig. 8). The HCl-leachates also contain minor but detectable amounts of Al, K, and Ti, indicating that the procedure also dissolved negligible amounts of aluminosilicates (Fig. 2; Dataset S1).

Our results suggest that barite was partly dissolved during the decarbonation, similar to observations in previous studies (e.g. Lyle et al., 1984; Tribovillard et al., 1996; Rutten and de Lange, 2002; Eagle et al., 2003; Gonneea and Paytan, 2006; see also Section 2.3). In the HCl-residues, linear relationships between Ba and Sr can only be observed for Group-A cores that contain little/no barite, showing the constant Sr/Ba ratio in detrital minerals (Fig. 4). While for Group-B and -C cores, the Ba-Sr data bifurcate between the barite-rich sapropel-S1 and the non-S1 samples, reflecting the different Sr/Ba ratios between detrital minerals and hydrogenetic barite (Fig. 4). Such contrasts explicitly suggest that barite and associated Sr remain in some of the decarbonated sapropel sediments (see also Section 4.1.2).

4.1.2. Barite extraction

Repeated leaching with NH_4Cl has proven to be adequate to extract barite in various marine sediments (Schenau et al., 2001; Rutten and de Lange, 2002; Reitz et al., 2004, 2006a; see also Section 2.3). In our study, the efficiency of barite extraction is clear. In the NH_4Cl-leachates for Group-A cores, some of the data are close to the analytical detection, causing the scattered distribution (Fig. 5; Table S2). By contrast, for Group-B and -C cores, the NH_4Cl-leachate samples contain considerable Ba and Sr in the sapropel S1 samples (Fig. 5). The barite-origin of the extracted phase is confirmed by 1) the good correlation of Ba-Sr in NH_4Cl-leachates observed for the Group-B and -C cores alone but not for

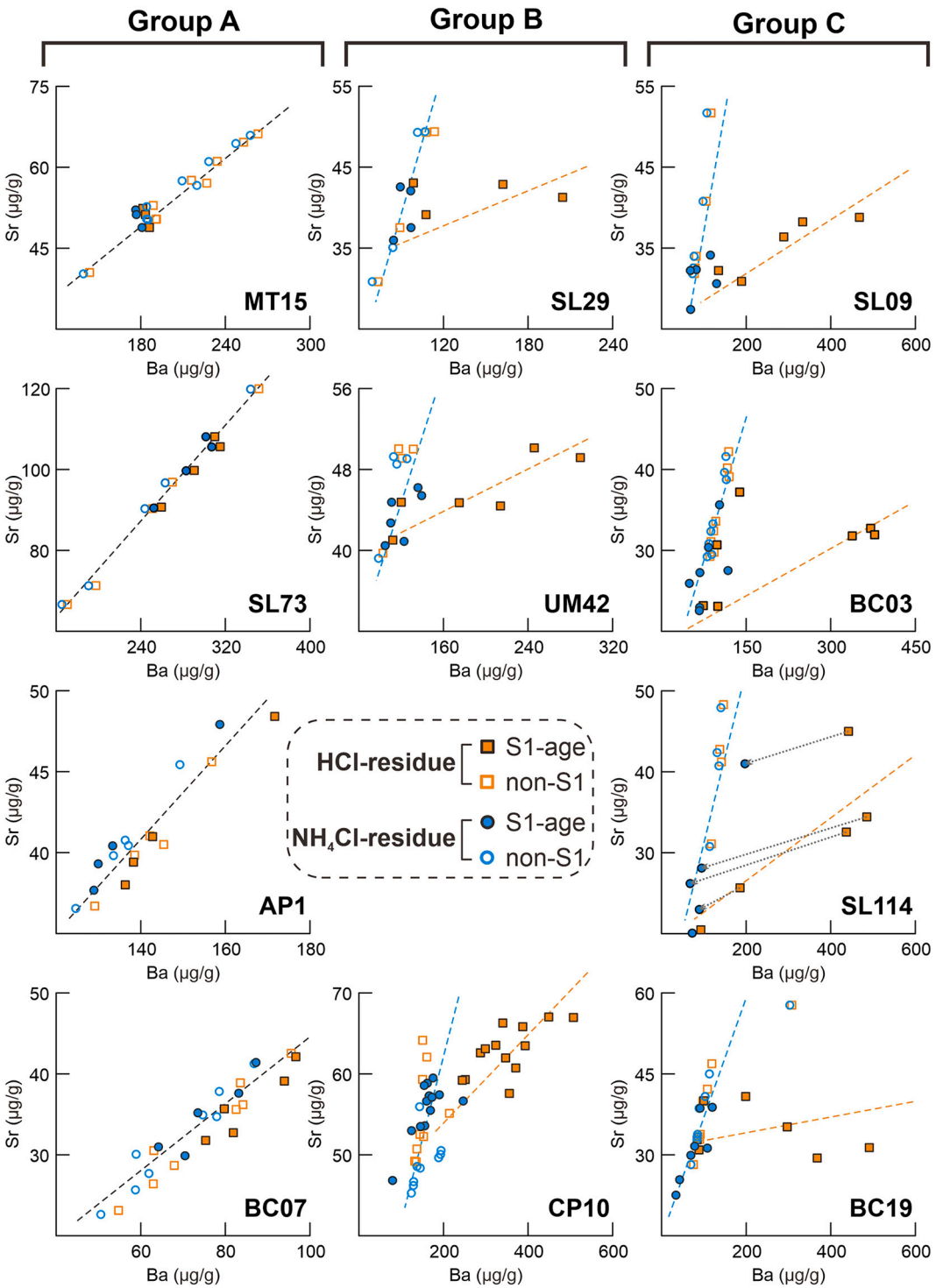

Fig. 4. Plots of Ba vs. Sr concentrations for the samples of HCl-residue (i.e. decarbonated sediments) and of NH_4Cl-resiude (i.e. carbonate- and barite-free sediments) (Table S2). The samples are distinguished between sapropel S1and non-S1. The potential existence of barite phase in decarbonated sediments is revealed – if applicable – by different trends (colored dashed lines) between HCl-residues and NH_4Cl-residues. The full removal of barite is illustrated by point-by-point links (gray dotted lines), as exemplified by core SL114 data. The cores are grouped by the barite-Ba contents of S1-aged bulk sediments: Group-A (<100–400 μg/g), Group-B (~200–800 μg/g), and Group-C (~300–1200 μg/g) (Section 4). Note the varying scales on the axes of different cores.

Group-A (Fig. 6), and 2) the Ba amounts in NH_4Cl-leachates are generally related to the bulk-Ba abundance, regardless of distinct provenance settings (Figs. S1–S3).

In particular, the complete dissolution of barite with the NH_4Cl-leaching procedure is evidenced by the linear correlation of Ba-Sr data in NH_4Cl-residues (Fig. 4). The correlation is observed for all the studied cores, regardless of the sample types, which suggests that the NH_4Cl-residue represents fully cleaned, i.e. all barite removed, detrital sediments. This is further corroborated by the differences between NH_4Cl-residues and HCl-residues (Fig. 4). In contrast to the strong Ba-Sr correlations in NH_4Cl-residue data, the HCl-residues show distinctly bifurcated patterns between S1 and non-S1 samples for the Group-B and

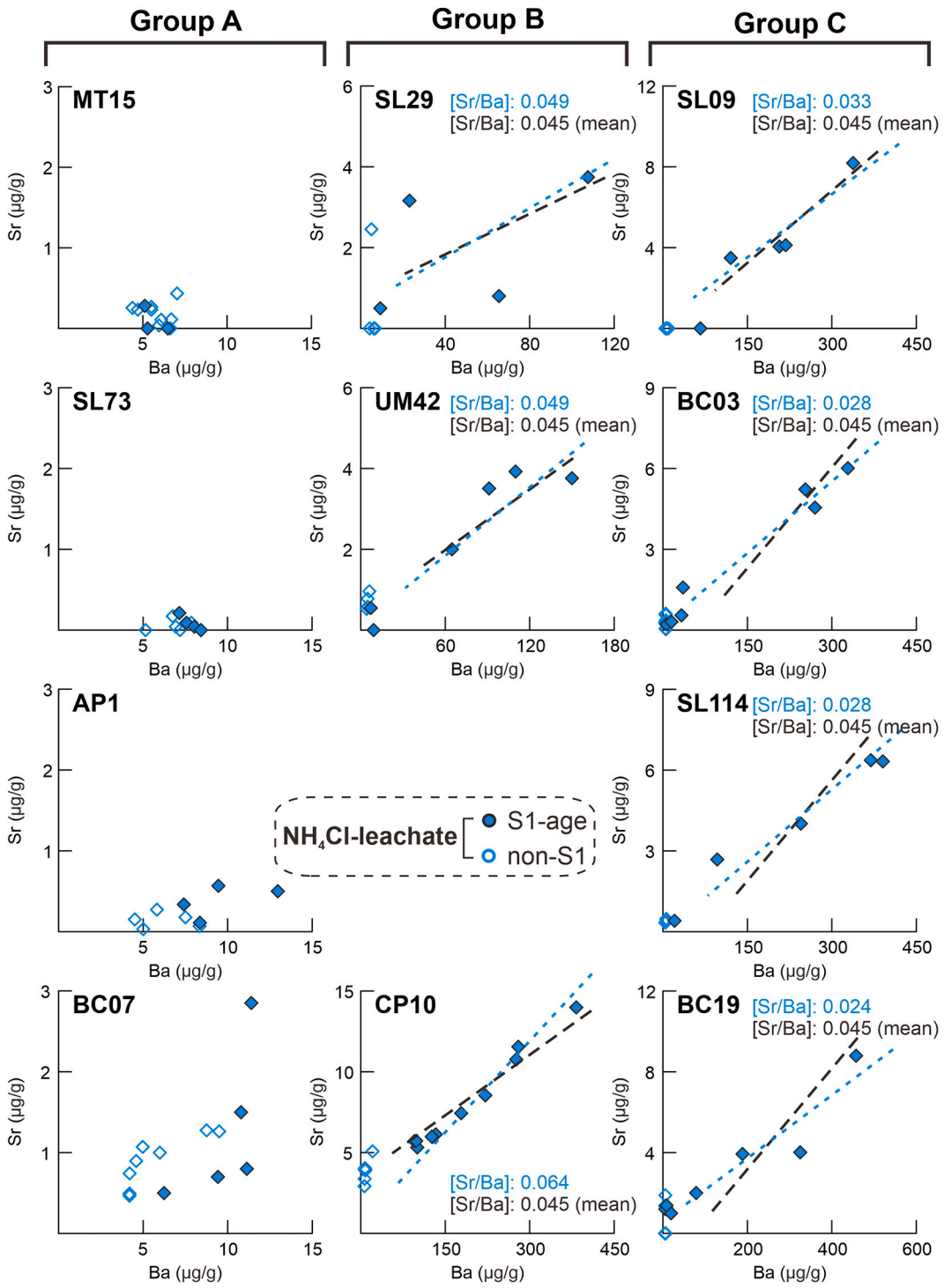

Fig. 5. Plots of Ba vs. Sr concentrations in the samples of NH_4Cl-leachate (i.e. barite-extracted solutions) (Table S2). The samples are distinguished between sapropel S1 and non-S1. Potentially extracted barite phases are depicted by dashed lines, corresponding to the molar ratios of Sr/Ba in barite (i.e. $[Sr/Ba]_{barite}$). For $[Sr/Ba]_{barite}$, both mean ratio (black dashed lines) and core-specific ratio (blue dashed lines) are shown – if applicable – as estimated from the NH_4Cl leaching results (see Fig. 6). For the Group-A samples having extremely low Ba and Sr, barite – if any – was dissolved in the preceding HCl decarbonation. The cores are grouped by the barite-Ba contents of S1-aged bulk sediments: Group-A (<100–400 µg/g), Group-B (~200–800 µg/g), and Group-C (~300–1200 µg/g) (Section 4). Note the varying scales on the axes of different cores.

-C cores (Fig. 4). This clearly reveals that barite-Sr potentially remaining in the HCl-residues had been removed, with the barite-free NH_4Cl-resiudes left.

Furthermore, the efficient NH_4Cl-leaching of barite is confirmed by the solely detrital composition in all NH_4Cl-residues. Firstly, the detrital origin for Ba and Sr in the NH_4Cl-residue is suggested by their linear correlations with Al (Dataset S1). Moreover, our results give a mean Ba/Al value of 0.0032 ± 0.0011 g/g (1σ, n = 33) for the carbonate- and barite-free sediments (i.e. NH_4Cl-residues; Table S1). This value is in good agreement with the reported values for the EMS aluminosilicate detritus (0.0027–0.0039 g/g; Rutten and de Lange, 2002; Reitz et al., 2004), and lower than the estimate of globally averaged crustal/shale

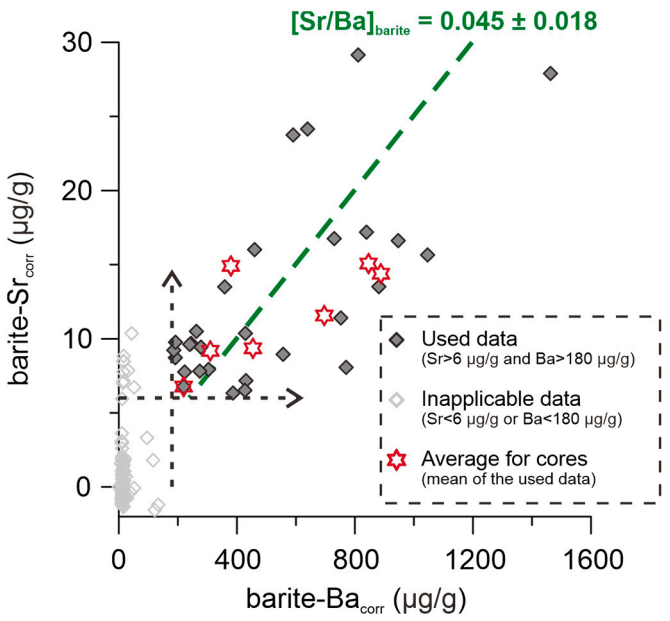

Fig. 6. The Ba and Sr data of NH_4Cl-leaching extracted phase of barite, corrected for a small fraction of dissolved aluminosilicates (i.e. barite-Ba_{corr} and barite-Sr_{corr}). The correction is done using the extracted Al and the mean values of Ba/Al (0.0032 g/g) and Sr/Al (0.0012 g/g) in NH_4Cl-residues as pristine detrital signatures (Table S2). The resultant barite Sr/Ba ratio for deep-sea Mediterranean sediments is: $(Sr/Ba)_{barite}$ = 0.029 ± 0.012 g/g (1σ, n = 29), equivalent to a molar ratio of $[Sr/Ba]_{barite}$ = 44.6 ± 18.4 mmol/mol (Table S2). Note that only the data with barite-Ba_{corr} > 180 µg/g and barite-Sr_{corr} > 6 µg/g considered excludes the samples with no/negligible barite and/or with larger procedural uncertainty. Core signatures are also specified if applicable. See Section 4.2.1 for details of correction and calculation.

Ba/Al ratios (0.005–0.01 g/g; Dymond et al., 1992; Klump et al., 2000; Robin et al., 2003; Reitz et al., 2004). In addition, the value for the primary detrital signature of Sr/Al (0.0012 ± 0.0003 g/g; 1σ, n = 33) in Mediterranean sediments is reported for the first time (Table S1).

Taken together, applying the sequential HCl- and NH_4Cl-leachings results in a complete removal of carbonate and barite, allowing the NH_4Cl-residues to be taken as the pure detrital phases (i.e. det-Ba, det-Sr).

4.2. Estimate of Ba- and Sr-bearing phases

4.2.1. Barite Sr/Ba ratio

Although variable amounts of barite may be dissolved during decarbonation, all remaining barite was clearly leached in the NH_4Cl filtrate (Figs. 4 and 5). Apart from barite, the barite extraction procedure may have dissolved minor amounts of detrital minerals, as seen from the minor amount of Al detected in the NH_4Cl-leachates (Fig. 2; Dataset S1). Although this detrital phase is quantitatively negligible, it might introduce errors to the calculated barite Sr/Ba values. Thus, the barite-Ba and barite-Sr values are corrected for the Ba and Sr of such potential detrital origin in the NH_4Cl-leachates using Eq. (3). In this equation, $(Ba/Al)_{detrital}$ and $(Sr/Al)_{detrital}$ refer to the basin-wide averaged values of Ba/Al (0.0032 g/g) and Sr/Al (0.0012 g/g) in the NH_4Cl-residues (i.e. carbonate- and barite-free sediments) (Table S1). Note the negligible difference in the final calculated values of barite Sr/Ba, if the core-specific values of $(Ba/Al)_{detrital}$ and $(Sr/Al)_{detrital}$ are used.

$$\text{barite-Ba}_{corr} = Ba_{NH4Cl-leachate} - Al_{NH4Cl-leachate} \times (Ba/Al)_{detrital} \quad (3a)$$

$$\text{barite-Sr}_{corr} = Sr_{NH4Cl-leachate} - Al_{NH4Cl-leachate} \times (Sr/Al)_{detrital} \quad (3b)$$

$$(Sr/Ba)_{barite} = \text{barite-Sr}_{corr}/\text{barite-Ba}_{corr} \quad (4)$$

Subsequently with Eq. (4), the typical barite Sr/Ba value is deduced for Mediterranean deep-sea sediments: $(Sr/Ba)_{barite}$ = 0.029 ± 0.012 g/g (1σ, n = 29), equivalent to a molar ratio $[Sr/Ba]_{barite}$ = 44.6 ± 18.4 mmol/mol (Fig. 6; Table S2). Note that only the data with barite-Ba_{corr} > 180 µg/g and barite-Sr_{corr} > 6 µg/g are taken into account (Fig. 6). These boundaries exclude the data from non-S1 samples that contain no barite (i.e. having low values and large errors) (Van Santvoort et al., 1996; Thomson et al., 1999; Martinez-Ruiz et al., 2000; see also Fig. 7).

As incomplete dissolution such as during decarbonation does not affect the relative concentration ratio in barite (Dehairs et al., 1980; Bishop, 1988; Averyt et al., 2003), our NH_4Cl-extraction must have preserved the geochemical composition of the barite phase. Therefore, the barite Sr/Ba ratio determined here reflects the initial barite composition. The Mediterranean deep-sea barite $[Sr/Ba]_{barite}$ ratio (44.6 ± 18.4 mmol/mol; this study) is relatively constant, which is consistent with those reported for the global ocean (~24–41 mmol/mol with mean value of 32.3 nmol/mol, Averyt and Paytan, 2003; ~31–56 mmol/mol with mean value of 41.0 nmol/mol, van Beek et al., 2003), and with the value derived for equatorial Pacific sediments (54.3 mmol/mol; Ziegler et al., 2007).

4.2.2. Different Ba-bearing phases

Sedimentary bulk-Ba is composed mainly of det-Ba and barite-Ba, while minor amounts of Ba potentially present in carbonate, organic matter, opal, and Fe-Mn oxides (Fig. 2; Table 2). A simple way of quantifying the barite content is to correct the total Ba in marine sediments for the non-barite, detrital contributions, determined from the empirical Ba/Al ratio for detrital aluminosilicates, as described in Eq. (5) (Dymond et al., 1992; Klump et al., 2000; Reitz et al., 2004; Bridgestock et al., 2019; see also Section 2.3). In Eq. (5), $(Ba/Al)_{detrital}$ refers to the detrital Ba/Al value as analyzed in the NH_4Cl-residue, either using a basin-averaged value (0.0032 g/g) for all Mediterranean cores, or using core-specific values (0.0015–0.0058 g/g) (see Section 4.1.2). This yields two datasets, barite-Ba#1 and barite-Ba#2 (Fig. 7).

Alternatively, the barite-Ba content (i.e. barite-Ba#3; Fig. 7) can be determined from our leaching results using Eq. (6), considering that the NH_4Cl-residue represents the detrital component alone with negligible amounts of Ba remaining in Fe-Mn oxides.

$$\text{barite-Ba} = Ba_{bulk-sediment} - Al_{bulk-sediment} \times (Ba/Al)_{detrital} \quad (5)$$

$$\text{barite-Ba} = Ba_{bulk-sediment} - Ba_{NH4Cl-residue} \quad (6)$$

The barite-Ba profiles calculated by the different methods show good correspondence for the barite-bearing Group-B and -C cores, while large differences occur for the Group-A cores that have minor/no barite (Fig. 7). Moreover, although the general patterns are similar, the profiles of barite-Ba#1 and #2 display outranged variations in some cores (i.e. MT15, BC07, SL29, UM42, SL09) (Fig. 7). This is probably caused by applying a constant detrital Ba/Al ratio to the different cores. Such errors would be especially large in the Mediterranean, receiving a huge quantity of detrital inputs from distinctly different source areas (Weldeab et al., 2002; Revel et al., 2010; Scheuvens et al., 2013; Wu et al., 2016, 2018; Blanchet et al., 2021; see also Section 2.1).

There seems to be minor barite-Ba during non-S1 intervals, which conflicts with the general notion that no barite formed in non-sapropel parts (Thomson et al., 1995, 1999; Van Santvoort et al., 1996; Martinez-Ruiz et al., 2000; Rutten and de Lange, 2002; Reitz et al., 2004). This difference is likely to be an artifact, caused by 1) taking a constant detrital Ba/Al value, basin-wide or core-specific and/or 2) neglecting the Ba hosted in carbonates and Fe-Mn oxides for the barite estimates (Lea and Boyle, 1989; Gingele and Dahmke, 1994; Robin et al., 2003; Gonneea and Paytan, 2006; Reitz et al., 2006a; see also Section 2.2). Ignoring these potential contributions may result in the non-zero backgrounds in barite-Ba profiles (Fig. 7). However, at this point we cannot fully rule out a minor barite presence in the pre- or post-S1 sediments.

Despite the minor uncertainties, the barite-Ba#3 appears to be the

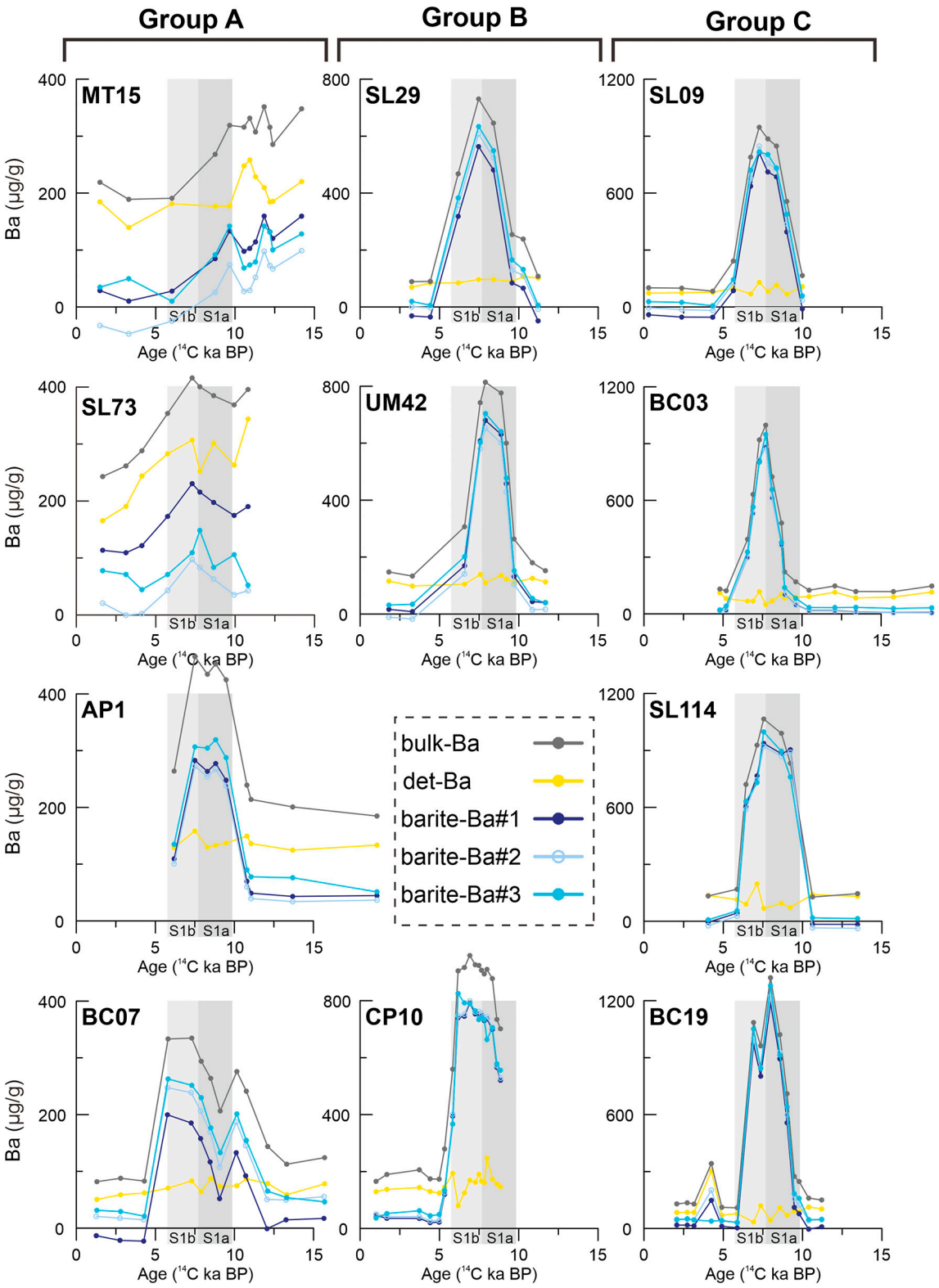

Fig. 7. Temporal records of different Ba phases over the S1-equivalent time, including those in bulk sediments (bulk-Ba), detrital minerals (det-Ba), and in the hydrogenetic components estimated by various methods (i.e. barite-Ba#1, barite-Ba#2, and barite-Ba#3) (Table S2). For the estimates of different Ba phases refer to Section 4.2.2. The barite-Ba#3 appears to be the best estimate of barite content for Mediterranean sediments. Sapropel S1 period (~9.8–5.7 ^{14}C ka; De Lange et al., 2008) and its sub-segments S1a and S1b (Rohling and Palike, 2005) are indicated. The cores are grouped by the barite-Ba contents of S1-aged bulk sediments: Group-A (<100–400 μg/g), Group-B (~200–800 μg/g), and Group-C (~300–1200 μg/g) (Section 4). Note that the horizontal axes are in conventional ^{14}C ages, and the scales of vertical axes vary between core-groups. (For interpretation of the references to colour in this figure legend, the reader is referred to the web version of this article.)

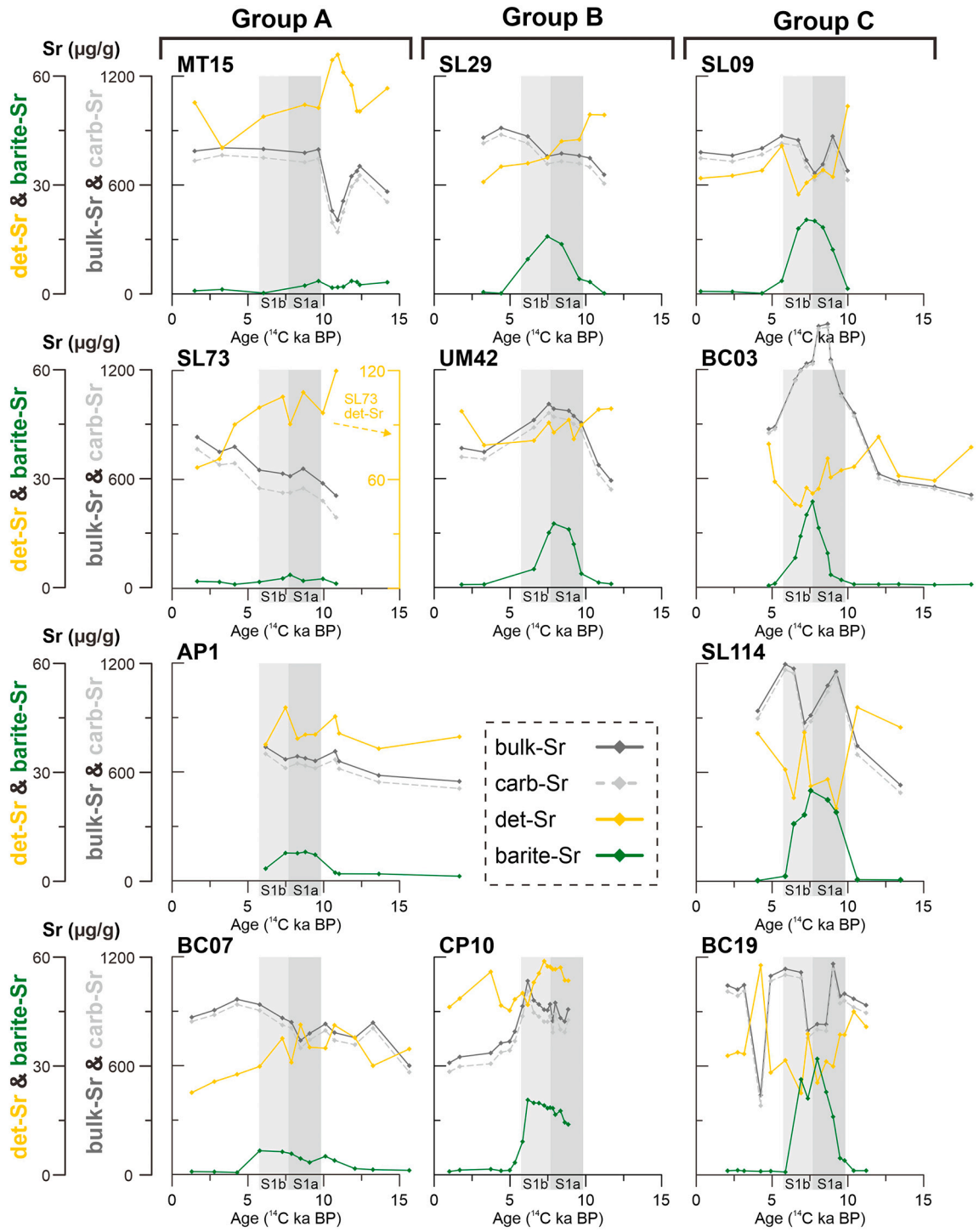

Fig. 8. Temporal records of different Sr phases over the S1-equivalent time, including those in bulk sediments (bulk-Sr), biogenic carbonates (carb-Sr), detrital minerals (det-Sr), and barite-bound (barite-Sr) estimated in this contribution (Table S2). For the estimates of different Sr phases refer to Section 4.2.3. Sapropel S1 period (~9.8–5.7 ^{14}C ka; De Lange et al., 2008) and its sub-segments S1a and S1b (Rohling and Palike, 2005) are indicated. Note that the horizontal axes are in conventional ^{14}C ages. The cores are grouped by the barite-Ba contents of S1-aged bulk sediments: Group-A (<100–400 μg/g), Group-B (~200–800 μg/g), and Group-C (~300–1200 μg/g) (Section 4). Note that the horizontal axes are in conventional ^{14}C ages, and the vertical axis differ for det-Sr of core SL73. (For interpretation of the references to colour in this figure legend, the reader is referred to the web version of this article.)

most appropriate method for reconstructing barite-Ba content and will be used in the following discussion (Fig. 7). The derived barite-Ba constitutes the major component (>60%) of the bulk-Ba during the sapropel S1 period, except for the shallowest core SL73 and the WMS core MT15. In the non-S1 intervals, the det-Ba dominates the variability of the bulk-Ba in marine sediments (Fig. 7). All the EMS cores show distinctly enhanced levels of bulk-Ba during the S1 period. This is mainly due to barite-Ba superimposed on the relatively stable background of det-Ba (Fig. 7). The degree of barite-Ba enhancement appears to correlate with water depth (Fig. 1; Table 1). This is consistent with previously observed enhanced levels of C_{org} and bulk-Ba for deeper EMS cores (Murat and Got, 2000; De Lange et al., 2008).

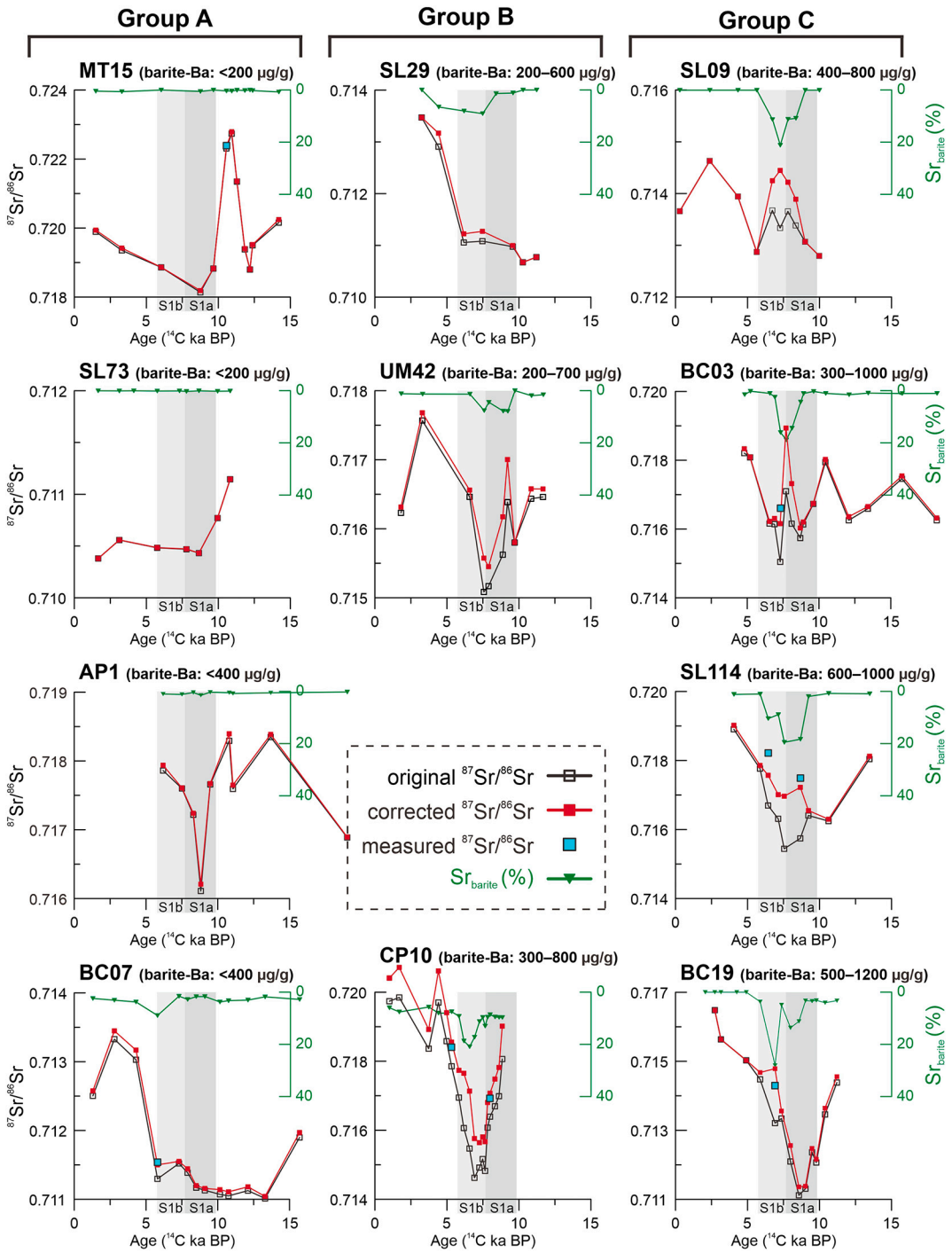

Fig. 9. Detrital $^{87}Sr/^{86}Sr$ records, comparing the originally reported data, data corrected using our leaching results, and data directly measured on carbonate- and barite-free sediments (i.e. NH_4Cl-residue) in this study (Tables S2 and S3). The Sr isotope ratios are corrected for potentially remaining barite-bound Sr in decarbonated sediments using Eq. (8). For correction details refer to Section 4.3. The errors of $^{87}Sr/^{86}Sr$ data are within symbols. For each core, the elevated level of barite-Ba content during sapropel S1 period is indicated. Sapropel S1 period (~9.8–5.7 ^{14}C ka; De Lange et al., 2008) and its sub-segments S1a and S1b (Rohling and Palike, 2005) are indicated. The cores are grouped by initial barite content in S1-aged bulk sediments (see Section 4). Note that the horizontal axes are in conventional ^{14}C ages, and the scales of vertical axes vary between core-groups. (For interpretation of the references to colour in this figure legend, the reader is referred to the web version of this article.)

4.2.3. *Different Sr-bearing phases*

In marine sediments, bulk-Sr consists mostly of carb-Sr, det-Sr, and barite-Sr (Fig. 2; Table 2). Here, carb-Sr and det-Sr refer to the Sr in the fractions of HCl-leachate and NH_4Cl-residue, respectively. The barite-Sr is calculated from barite-Ba and multiplied by the Mediterranean barite Sr/Ba signature (0.029 g/g) using Eq. (7). The use of a constant Sr/Ba ratio is supported by the narrow ranges reported globally for deep-sea barite (Averyt and Paytan, 2003; van Beek et al., 2003; Ziegler et al., 2007; this study) (Fig. 6; see also Section 4.2.1).

$$\text{barite-Sr} = \text{barite-Ba} \times (\text{Sr/Ba})_{\text{barite}} \quad (7)$$

Temporal records of different Sr phases are plotted in Fig. 8. The carb-Sr dominates the bulk-Sr for all the cores (>80%), while the det-Sr and barite-Sr have minor contribution (Fig. 8). The derived barite-Sr

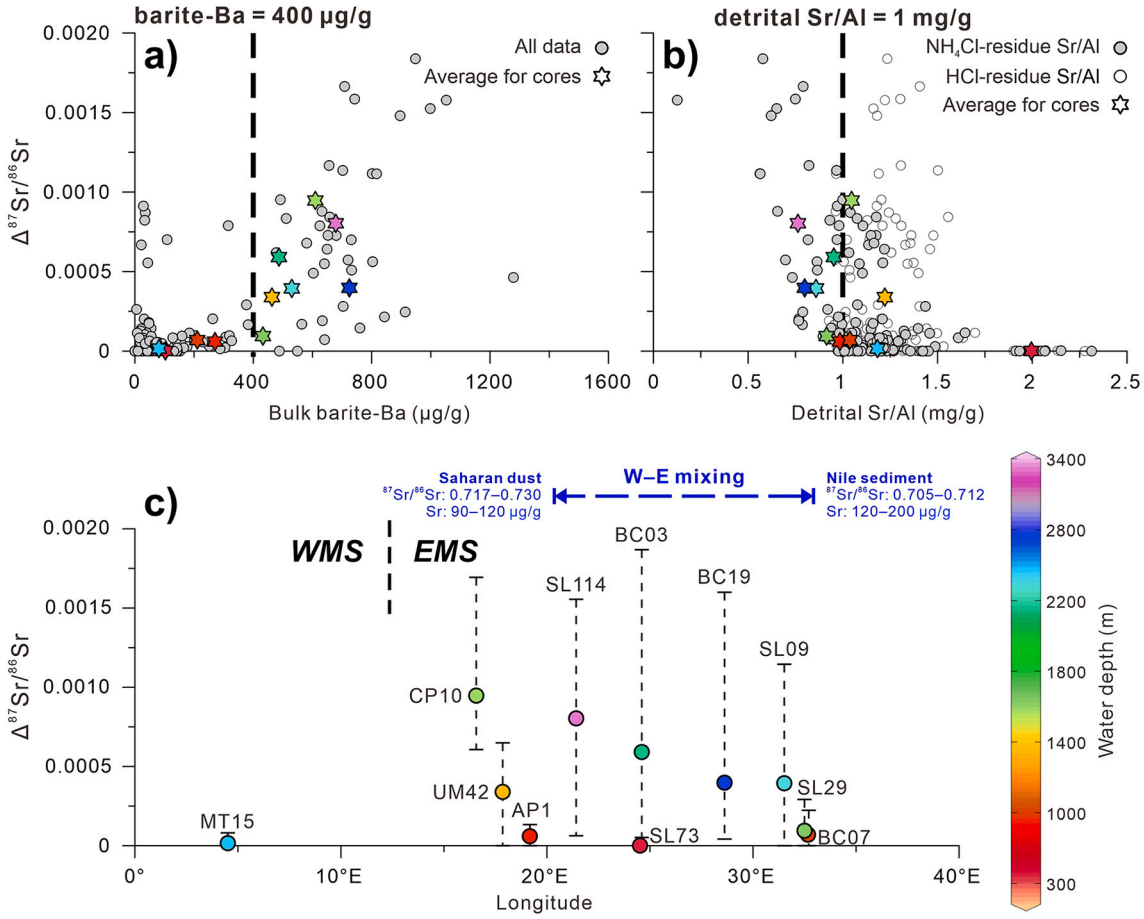

Fig. 10. Exemplifying the factors influencing barite-Sr effect from Mediterranean sediments. Difference between corrected and uncorrected $^{87}Sr/^{86}Sr$ ratios ($\Delta^{87}Sr/^{86}Sr$) versus a) bulk barite-Ba content, b) detrital Sr/Al ratio, and c) longitude of the studied cores. The $^{87}Sr/^{86}Sr$ correction of barite-Sr refers to Section 4.3 (Fig. 9). The bulk barite content after the estimate of barite-Ba#3 (Fig. 7; see also Section 4.2) (a). The detrital Sr/Al ratios are on the carbonate- and barite-free NH4Cl-residues, with the ratios of HCl-residues compared (Table S1; see Section 4.1) (b). For sapropel S1-period interval that potentially contains barite, average values and associated ranges are shown for each core (c). Core symbols are specified by colors according to water depth, given the general correlation between barite content and water depth (Figs. 1 and 7). The barite-Sr effect (i.e. $\Delta^{87}Sr/^{86}Sr$) become prominent with barite-Ba >400 μg/g in bulk sediments. This effect would be more prominent if accompanied by high $^{87}Sr/^{86}Sr$ (>0.713) or low Sr/Al (<1.0 mg/g) in terrigenous detrital component. Due to the west–east gradients in $^{87}Sr/^{86}Sr$ and Sr concentration caused by a mixing between Nile and Saharan contributions, cores SL114 and CP10 that are in the deep-sea basins and in the western parts of the EMS show the largest $^{87}Sr/^{86}Sr$ deviations. See Section 5.1 for interpretations. (For interpretation of the references to colour in this figure legend, the reader is referred to the web version of this article.)

contents are strongly correlated with bulk-Ba contents (Fig. 7; see also Figs. S1–S3).

4.3. Correction of $^{87}Sr/^{86}Sr$ data of decarbonated sediments

Based on the leaching results, we can correct the Sr isotope ratio of decarbonated sediments for the remaining barite-bound Sr, using Eq. (8). Therein, $^{87}Sr/^{86}Sr_{barite}$ is the marine-barite $^{87}Sr/^{86}Sr$ value reported for the deep-sea Mediterranean seawater (0.709165; De Lange et al., 1990), which is similar to that of modern oceanic marine-barite (0.709175; Paytan et al., 1993). The Sr_{barite} is the percentage of barite-bound Sr remaining in decarbonated sediments, i.e. $Sr_{barite} = (1 - \text{det-Sr} / (\text{bulk-Sr} - \text{carb-Sr})) \times 100\% = (1 - Sr_{NH4Cl\text{-}residue} / Sr_{HCl\text{-}residue}) \times 100\%$ (Table S2).

$$^{87}Sr/^{86}Sr_{corrected} = \left(^{87}Sr/^{86}Sr_{original} - ^{87}Sr/^{86}Sr_{barite} \times Sr_{barite}\right) \Big/ (1 - Sr_{barite}) \quad (8)$$

Overall, application of the correction not only changes the absolute values of $^{87}Sr/^{86}Sr$ but also alters the temporal variability in several cores (Fig. 9). The corrected $^{87}Sr/^{86}Sr$ ratios are systematically higher than (or equal to) the uncorrected ratios, with differences (i.e. $\Delta^{87}Sr/^{86}Sr$) up to 0.001838 (Table S2). This is because the Sr isotope signature of marine barite ($^{87}Sr/^{86}Sr$: 0.709165–0.709175; De Lange et al., 1990; Paytan et al., 1993) is lower than that of most terrigenous inputs from the circum-Mediterranean region ($^{87}Sr/^{86}Sr$: ~0.705–0.730; cf. Krom et al., 1999; Weldeab et al., 2002; Revel et al., 2010; Scheuvens et al., 2013; Wu et al., 2016). After correction, detectable alterations in $^{87}Sr/^{86}Sr$ record occur only within the sapropel interval (Fig. 9). The $\Delta^{87}Sr/^{86}Sr$ appears negligible for the Group-A cores with little/no barite, while it is considerable in Group-B and -C cores that have a more elevated level of bulk barite during the S1-period (Fig. 9).

4.3.1. Verifying the Sr isotope correction

The Sr isotopes were directly measured on a representative selection of NH_4Cl-residue samples to verify the correction of decarbonated-sediment $^{87}Sr/^{86}Sr$ data (Fig. 9; Table S3). The same (within error) $^{87}Sr/^{86}Sr$ ratios between uncorrected, corrected, and measured values are obtained for Group-A cores (i.e. MT15 and BC07) (Fig. 9). Representative for Group-B, core CP10 records a large change in $^{87}Sr/^{86}Sr$ ratio inferred by the applied correction ($\Delta^{87}Sr/^{86}Sr$: ~0.000641–0.001640), but shows nearly identical results between the corrected and directly analyzed $^{87}Sr/^{86}Sr$ values (i.e. differences <0.000149) (Fig. 9; Table S3). This close correspondence confirms the

reliability of the total procedures and data analyses.

For Group-C cores, Sr-isotope analyses were only realized on the samples that are largely affected by barite-Sr correction (i.e. $\Delta^{87}Sr/^{86}Sr > 0.001$) (Table S3). Although the measured and corrected data are not always identical (i.e. differences <0.000485), all directly measured $^{87}Sr/^{86}Sr$ ratios are consistent with the direction of changes in corrected data (Fig. 9). That is, all corrected $^{87}Sr/^{86}Sr$ ratios are >0.001093 higher than the uncorrected values, shifting away from the modern seawater signature. This certifies the general usefulness of a barite-Sr related correction on the $^{87}Sr/^{86}Sr$ data of decarbonated sediments.

Notably, the required correction appears to have larger uncertainty for the samples with >1000 μg/g bulk barite-Ba (Table S3). For cores BC03 and SL114, the analyzed $^{87}Sr/^{86}Sr$ ratios of NH_4Cl-residue samples are higher than the corrected ratios, while the reverse is the case for core BC19 (Fig. 9). Such uncertainties necessitate a direct analytical removal of barite for barite-rich samples.

5. Discussion and implications

Taking Mediterranean sediments as pertinent examples, our results reveal the potential importance of residual barite and associated Sr in decarbonated sediments. This is evidenced by a combination of 1) amounts of Ba and Sr dissolved in the NH_4Cl-leachates and 2) concurrent changes in the Ba-Sr data, showing a shift from the bifurcated relationships (i.e. detrital and barite) in HCl-residues to the linear correlation (i.e. detrital only) in NH_4Cl-residues (Figs. 4 and 5). These observations are limited to the barite-rich samples from sapropel layers. In addition, the amount of remaining barite is proportional to the barite content of the initial bulk sediment (Figs. 7 and 8). Specifically, the remaining barite is negligible for Group-A cores having <100–400 μg/g bulk barite-Ba, while considerable for Group-B and -C cores that are characterized by elevated barite-Ba levels of ~200–800 μg/g and ~300–1200 μg/g, respectively, in sapropel S1 interval (Fig. 9).

We first exemplify the factors influencing the barite-Sr effect for Mediterranean sediments (Section 5.1). From a wider perspective, the pertinent case of the Mediterranean is compared with other high-productivity settings, with new insights and global implications given (Section 5.2). Finally, we propose an improved protocol for the adequate separation of detrital Sr, applicable for all barite-containing sediments (Section 5.3).

5.1. Barite-Sr effect in Mediterranean sediments

There are two factors influencing the barite-Sr effect on the "detrital" Sr isotope signal derived from samples with incompletely removed barite: sediment barite content, and detrital Sr composition of provenance.

The role of barite is evident from the observation that barite-bound Sr only occurs in the barite-rich sapropel samples (Fig. 8). Moreover, being indicative of the barite-Sr effect, $\Delta^{87}Sr/^{86}Sr$ becomes obvious when the bulk barite-Ba content exceeds 400 μg/g, showing a trend of positive correlation (Fig. 10a). This threshold specifies a ratio of Ba/Al >8.8 mg/g for average Mediterranean sediment Al content of 4.6% (Dataset S1). Additionally, given the positive correlation between the elevated level of bulk barite-Ba and the water depth of the EMS cores (Figs. 1 and 7), the threshold of 400-μg/g barite-Ba corresponds to a boundary of ~1000 m water depth in the EMS (Figs. 9 and 10c).

The barite-Sr effect also depends on provenance background, including 1) detrital Sr content in the sediment, and 2) the difference in $^{87}Sr/^{86}Sr$ ratio between the terrigenous detritus and contemporary seawater. In other words, after the correction of seawater-derived barite, larger deviation in $^{87}Sr/^{86}Sr$ data would occur if the detrital component has a lower Sr concentration, or a larger $^{87}Sr/^{86}Sr$ offset from the seawater ratio (modern seawater $^{87}Sr/^{86}Sr$: 0.709165–0.709175; De Lange et al., 1990; Paytan et al., 1993).

As shown in Fig. 10b, the $\Delta^{87}Sr/^{86}Sr$ substantially increases when the detrital Sr/Al ratio is below 1.0 mg/g. It must be noted that this subtle trend can only be discerned from the data of NH_4Cl-residues, but not observed for HCl-residues (Fig. 10b). This, in turn, highlights the use of fully cleaned, i.e. carbonate- and barite-free detrital sediments for provenance studies.

For the Mediterranean, there is a mixing between Nile sediments ($^{87}Sr/^{86}Sr$: ~0.705–0.712; Sr: ~120–200 μg/g) diluted towards the west by Saharan dust ($^{87}Sr/^{86}Sr$: ~0.717–0.730; Sr: ~90–120 μg/g) (cf. Krom et al., 1999; Freydier et al., 2001; Weldeab et al., 2002; Revel et al., 2010; Wu et al., 2016, 2018). This mixing is manifested in our basin-wide coverage, showing generally higher $^{87}Sr/^{86}Sr$ in more western areas (Figs. 1 and 9). Such a west–east gradient is also clearly seen from the Sr/Al and Ba/Al ratios in the NH_4Cl-residue samples (Table S1). Consequently, the inferred effect is amplified in the western but subdued in the eastern part of the EMS (Fig. 10c).

Taken together, the impact of barite-Sr should be prominent for cores 1) in the EMS deep-sea basins (i.e. abundant barite in bulk sediment) and 2) in the western parts of the EMS (i.e. high $^{87}Sr/^{86}Sr$ and low Sr/Al of provenance background) (Figs. 1 and 10). The largest $\Delta^{87}Sr/^{86}Sr$ values are observed for cores SL114 and CP10. Both cores contain 500–1000 μg/g of barite-Ba in S1 sediments and are located in the Ionian Sea that has a rather radiogenic $^{87}Sr/^{86}Sr$ (~0.716–0.717) (Figs. 9 and 10). Core UM42 appears to be affected by both factors, but to a much lesser extent (S1-sediment barite-Ba: ~200–700 μg/g; $^{87}Sr/^{86}Sr$ background: ~0.715–0.716) (Figs. 9 and 10). Cores SL09, BC03, and BC19 – collected from the Levantine Basin – show considerable deviations in $\Delta^{87}Sr/^{86}Sr$, mainly due to the enhanced levels of barite-Ba: (~300–1200 μg/g) that are nevertheless buffered by the Nile-dominated $^{87}Sr/^{86}Sr$ background (~0.711–0.716) (Figs. 9 and 10). Minor impact is seen for cores BC07, AP1, SL73, and MT15 with little/no barite (S1-sediment barite-Ba: <100–400 μg/g) independent of their respective locations (Figs. 9 and 10).

At a closer look, the $\Delta^{87}Sr/^{86}Sr$ shift as observed for cores SL09 and BC19 may depict the distribution limit of the Nile sediment discharge (Fig. 10c). This geographical mark gives a boundary value of $^{87}Sr/^{86}Sr > 0.713$ on terrigenous detrital background for a discernable effect of barite-Sr (Fig. 9). Moreover, the $^{87}Sr/^{86}Sr$ value of 0.713 coincides with that of the present-day average flux-weighed river input to the ocean (Pearce et al., 2015; Paytan et al., 2021). Therefore, this criterion should be valid for the whole Quaternary considering the long oceanic residence time of Sr (~2.4 Ma; Vance et al., 2009; Krabbenhöft et al., 2010).

Not only barite and provenance factor may play a role, but also the way that detrital Sr isotope systematics are applied. The coupled use of $^{87}Sr/^{86}Sr$ with Nd isotopes that are conservative in most sedimentary processes would seemingly "diminish" the differences between uncorrected and corrected data (Fig. S4). By contrast, the deviations deteriorate when Sr isotope systematics is used alone, such as in the classical discrimination of $^{87}Sr/^{86}Sr$ vs. 1000/Sr (e.g. Grousset et al., 1998; Krom et al., 1999; Stein et al., 2007; Box et al., 2011; Wu et al., 2016) (Fig. S5). For details see Supporting Information.

5.2. Global implications for high-productivity regions or time intervals

Our NH_4Cl-leaching has removed the barite remaining after decarbonation and thus yielded the "pure" primary detrital component (Figs. 4 and 5). For the first time, a ratio of $[Sr/Ba]_{barite}$ (44.6 ± 18.4 mmol/mol) is estimated for the Mediterranean sapropel sediments (Fig. 6). This ratio is comparable to the average values of barite reported in the recent global ocean (40.1 ± 12.2 mmol/mol; Averyt and Paytan, 2003; van Beek et al., 2003) and derived for equatorial Pacific sediments (54.3 mmol/mol; Ziegler et al., 2007).

Some barite dissolves during decarbonation; and the dissolved fraction is calculated (i.e. 1 – $Sr_{NH4Cl\text{-}leachate}$ / barite-Sr) (Table S2; see also Figs. S1–S3). The Group-A cores with negligible barite give a dissolved fraction of ~94% with large errors, whereas the other cores yield values of between 70–84%, except a mean value of ~55% for core CP10

(Table S2). The distinct data of CP10 may reflect a variable Sr/Ba ratio or Sr content of the barite precipitates, which should be partly responsible for the outlier data-points (i.e. high $\Delta^{87}Sr/^{86}Sr$ with little/no barite-Ba) in Fig. 10a. Such variability has been related to barite morphology and its various formation stages (Bishop, 1988; Bertram and Cowen, 1997; Rushdi et al., 2000; Martinez-Ruiz et al., 2019), and environmental conditions where barite formed (Averyt and Paytan, 2003; van Beek et al., 2003; Widanagamage et al., 2015). Recently, an experimental study has shown that barite crystallites incorporate more Sr when organic films are present (Deng et al., 2019a). This issue is certainly a target for future studies.

The inferred barite-Sr effect is probably more prominent in other areas, as exemplified below. Firstly, our decarbonation is more rigorous than some other methods used in marine-sediment provenance studies. A combination of stronger acid (1 M HCl compared to acetic acid), longer and repeated treatments, and the higher ratio of acid to sample ensures a full removal of carbonate (Van Santvoort et al., 1996; Wu et al., 2017) (Section 3.2.1). For the less aggressive methods – if fully removing the carbonate – more barite could remain in the decarbonated sediments, resulting in a higher fraction of barite-Sr and a larger deviation from the true detrital Sr and $^{87}Sr/^{86}Sr$ ratios.

Secondly, in our case, enhanced barite is always accompanied by a shift in detrital provenance to higher Sr/Al and lower $^{87}Sr/^{86}Sr$ (i.e. towards the seawater ratio), given the reduced Saharan dust and increased Nile input during humid sapropel periods (Figs. 9 and 10; see also Section 2.1). In other words, the barite-Sr effect is compensated by a provenance change in the Mediterranean. But this may not be the case elsewhere. For instance, the circum-Antarctic regions are characterized by abundant barite in the surface sediments (i.e. barite-Ba and/or excess Ba commonly range in 500–6000 μg/g; Eagle et al., 2003; Jaccard et al., 2010, 2013; Planchon et al., 2013), and by a relatively radiogenic provenance background of detrital $^{87}Sr/^{86}Sr$ (~0.710–0.745; Walter et al., 2000; Hemming et al., 2007; Rutberg et al., 2005) at the same time.

Moreover, pronounced glacial–interglacial variability was found in the circum-Antarctic regions, showing that higher Ba/Al and higher $^{87}Sr/^{86}Sr$ simultaneously occurred during the warmer climate intervals (i.e. interglacial), and vice vera (Rutberg et al., 2005; Jaccard et al., 2010, 2013). Consequently, the derived detrital Sr composition for the Southern Ocean should be highly susceptible to the barite-Sr effect. Similar scenarios also may take place in the areas proximal to continental margin (e.g. Dymond et al., 1992; Fagel et al., 1999; Klump et al., 2000; Schenau et al., 2001), which have high barite content in the sediments, and drastic variations in detrital provenance through time (e.g. caused by sea level change).

Finally, barite fluxes to sapropel sediments are relatively low compared to those in many oceanic high-productivity regions or time intervals. Barite-Ba fluxes of ~0.5–2.5 mg/cm^2/ka have been shown for the basin-wide EMS during the S1-period (De Lange et al., 2008). By contrast, the Southern Ocean has a ^{230}Th-normalized bio-Ba flux of ~0.7–2.5 mg/cm^2/ka for the Holocene, and this flux increases 5 times (i.e. ~4–12 mg/cm^2/ka) during the last interglacial maximum (Jaccard et al., 2010, 2013). Likewise, a benthic Ba flux of ~4–7.5 mg/cm^2/ka was suggested for the biologically active upwelling zones of the equatorial Pacific (Paytan and Kastner, 1996), and this present-day flux may double during glacial times (Paytan et al., 1996).

For the eastern equatorial Pacific, in fact, possible persistence of barite in the residue after various leaching has been noted via the strong correlation between the excess Sr and excess Ba being ~2000–16,000 μg/g (Ziegler et al., 2007). In this high-productivity region, our inferences are further supported by a comparison between the samples with and without a treatment of chelating solution to dissolve barite (Xie and Marcantonio, 2012). After the treatment that may not fully remove barite, detrital $^{87}Sr/^{86}Sr$ shift away from the modern seawater signature by ~0.0001 to less radiogenic ratios, and this shift is larger for glacial than for interglacial samples (Xie and Marcantonio, 2012). Despite the opposite shifting direction to our case of Mediterranean sediments (Fig. 9) which is caused by the contrasting provenance backgrounds relative to the modern seawater, the magnitude of the $^{87}Sr/^{86}Sr$ changes is consistent with our results and extrapolation.

Furthermore, the inferred effect of barite-Sr is likely to have occurred in the geological past, such as the Paleocene–Eocene thermal maximum (PETM), and the Cretaceous oceanic anoxic events (OAE) and associated black shales (e.g. Paytan et al., 2002; Ma et al., 2014; Bridgestock et al., 2019), which all have significant high barite accumulation (cf. Paytan and Griffith, 2007).

5.3. Recommendation to improve separation of detrital Sr

The data presented here demonstrate that more caution is required for results and interpretations of "detrital" Sr systematics in the presence of sedimentary barite. Although a "normative" correction for the potential barite-Sr effect would be beneficial to the bulk data of Sr isotopes previously done on decarbonated sediments, it is difficult to draw an adequate empirical formula from our results. This is mainly due to insufficient knowledge on the variability of barite Sr/Ba and Sr content that is tightly related to barite formation and dissolution (cf. Deng et al., 2019a; Martinez-Ruiz et al., 2019), and partly because of the uncertainties discussed above (see also Section 4.3.1).

All uncertainties for a normative correction strongly prompt for methodological improvements in the separation of detrital Sr. A simple and effective way is adding a step of NH_4Cl leaching (2 M, pH 7) – repeated if needed – to fully remove barite and associated Sr after decarbonation. Detailed results using the BASEX method have indicated that most Ba extractable in this solvent was extracted in the first two leaches (Rutten and de Lange, 2002). Hence, the additional NH_4Cl leaching is practical and ensures a fully cleaned, barite-free component for the studies using detrital Sr systematics. This procedure is especially required for high-productivity areas and time intervals characterized by abundant barite in marine sediments. These include the Southern Ocean, equatorial Pacific, Arabian Sea, as well as the deep geological time of the PETM and OAEs and associated black shales (see Section 5.2).

Notably, the suggested procedure is applicable for both radiogenic and stable Sr isotopes. In fact, residual barite-Sr is expected to have a more critical impact on the $\delta^{88/86}Sr$ results (e.g. Krabbenhöft et al., 2010; Wei et al., 2013; Pearce et al., 2015; Stevenson et al., 2018; Paytan et al., 2021).

We recommend that, for all relevant studies, the additional step of NH_4Cl leaching is performed – at least – on representative samples to assess the potential barite impact. Subsequently, the derived results can be applied to the full sample set.

6. Concluding remarks

Provenance and weathering investigations often assume that acid-leaching on marine sediments fully removes the hydrogenetic, non-detrital components, with the residues being considered all detrital in origin. However, acceptance of this pathway is largely a result of insufficient knowledge on the geochemical behavior – especially the dissolution effects – of marine barite, which is characterized by abundant Sr and seawater-derived $^{87}Sr/^{86}Sr$ composition.

Using Mediterranean sediments for an exemplary study, we demonstrate the existence of remaining barite and associated Sr after traditional carbonate removal. If detrital Sr systematics in marine sediments is evaluated, then this must be taken into account. The barite-bound Sr becomes prominent when marine sediments have >400 μg/g barite-Ba contents and, as such, an adequate correction is necessary. This is particularly required if the enhanced barite occurs in sediments characterized by a terrigenous detrital background of high $^{87}Sr/^{86}Sr$ ratios (>0.713) or low Sr/Al ratios (<1.0 mg/g). If barite-Sr with a typical low seawater $^{87}Sr/^{86}Sr$ (~0.7091) is mixed with detrital Sr isotope and elemental composition, obviously, such mixture does not

represent the pure detrital signal.

From a global perspective, we stress that decarbonation alone may jeopardize the use of detrital Sr systematics (including radiogenic and stable Sr isotopes and Sr content) as diagnostic tool for provenance and weathering studies. More caution and even re-consideration may be required for previous Sr-isotope studies on detrital sediments. An improved protocol for preparing the pure detrital Sr component is proposed for future studies on marine sediments, with a NH_4Cl (2 M, pH 7) leaching step to remove barite and associated Sr potentially remaining after decarbonation. This protocol is especially recommended for high-productivity regions and/or time intervals that potentially have a high sedimentary barite content.

Declaration of Competing Interest

The authors declare no competing interests.

Acknowledgements

Many thanks are given to the captain & crew, scientists & technicians on board the cruises listed in Table 1 for core collections. We are indebted to Anja Reitz, Arrian Rutten, Caroline Slomp, David Gallego-Torres, Enno Schefuß, Patrick van Santvoort, Rinske Knoop, and Sanela Gusic for sediment processing and data analyses. We also thank Dineke van de Meent-Olieman, Helen de Waard, Ton Zalm, and Coen Mulder at Utrecht, Peijun Qiao, Hui Li, Pengfei Liu, Juan Xu at Tongji, as well as Richard Smeets and Mathijs van de Ven at VU Amsterdam for laboratory assistance and analyses. Philipp Böning and Caroline Slomp are acknowledged for comments on an earlier manuscript. We are grateful for the critical but constructive comments given by Matthew Fantle and six anonymous reviewers that all were very useful to improve our initial manuscripts. The efficient handling and guideline of Editor-in-Chief Michael Böttcher are highly appreciated. This work is financially supported by National Key R&D Program of China (2018YFE0202402), National Natural Science Foundation of China (41806064, 42006060), and China Postdoctoral Science Foundation (2019T120352, 2018M640418). European Programmes MARFLUX (MAST1-90022C), PALEOFLUX (MAS2-CT93-0051), and SAP (MAS3-CT97-0137) are acknowledged for partially funding the cruises. The shiptime and logistics granted by CNR and NWO are appreciated. This study is part of JW's PhD project, funded by the CSC–UU PhD Program (CSC No. 201206260116; USES contribution 146).

Appendix A. Supplementary data

Supplementary data to this article can be found online at https://doi.org/10.1016/j.chemgeo.2021.120613.

References

Averyt, K.B., Paytan, A., 2003. Empirical partition coefficients for Sr and ca in marine barite: Implications for reconstructing seawater Sr and Ca concentrations. Geochem. Geophys. Geosyst. 4, 1043. https://doi.org/10.1029/2002GC000426.

Averyt, K.B., Paytan, A., Li, G.C., 2003. A precise, high-throughput method for determining Sr/Ca, Sr/Ba, and Ca/Ba ratios in marine barite. Geochem. Geophys. Geosyst. 4, 1039. https://doi.org/10.1029/2002GC000467.

Bao, H., 2006. Purifying barite for oxygen isotope measurement by dissolution and reprecipitation in a chelating solution. Anal. Chem. 78, 304–309.

Bayon, G., German, C.R., Boella, R.M., Milton, J.A., Taylor, R.N., Nesbitt, R.W., 2002. An improved method for extracting marine sediment fractions and its application to Sr and Nd isotopic analysis. Chem. Geol. 187, 179–199.

Benkovitz, A., Matthews, A., Teutsch, N., Poulton, S.W., Bar-Matthews, M., Almogi-Labin, A., 2020. Tracing water column euxinia in Eastern Mediterranean Sapropels S5 and S7. Chem. Geol. 545, 119627.

Bernstein, R.E., Byrne, R.H., Betzer, P.R., Greco, A.M., 1992. Morphologies and transformations of celestite in seawater: the role of acantharians in strontium and barium geochemistry. Geochim. Cosmochim. Acta 56, 3273–3279.

Bernstein, R.E., Byrne, R.H., Schijf, J., 1998. Acantharians: a missing link in the oceanic biogeochemistry of barium. Deep-Sea Res. Part I Oceanogr. Res. Papers 45, 491–505.

Bertram, M.A., Cowen, J.P., 1997. Morphological and compositional evidence for biotic precipitation of marine barite. J. Mar. Res. 55, 577–593.

Bishop, J.K.B., 1988. The barite-opal-organic carbon association in oceanic particulate matter. Nature 332, 341–343.

Blanchet, C.L., Osborne, A.H., Tjallingii, R., Ehrmann, E., Friedrich, T., Timmermann, A., Brückmann, W., Frank, M., 2021. Drivers of river reactivation in North Africa during the last glacial cycle. Nat. Geosci. 14, 97–103.

Blum, J.D., Erel, Y., 1995. A silicate weathering mechanism linking increases in marine $^{87}Sr/^{86}Sr$ with global glaciation. Nature 373, 415–418.

Box, M.R., Krom, M.D., Cliff, R.A., Bar-Matthews, M., Almogi-Labin, A., Ayalon, A., Paterne, M., 2011. Response of the Nile and its catchment to millennial-scale climatic change since the LGM from Sr isotopes and major elements of East Mediterranean sediments. Quat. Sci. Rev. 30, 431–442.

Bridgestock, L., Hsieh, Y.T., Porcelli, D., Henderson, G.M., 2019. Increased export production during recovery from the Paleocene-Eocene thermal maximum constrained by sedimentary Ba isotopes. Earth Planet. Sci. Lett. 510, 53–63.

Church, T.M., Wolgemuth, K., 1972. Marine barite saturation. Earth Planet. Sci. Lett. 15, 35–44.

Cole, J.M., Goldstein, S.L., DeMenocal, P.B., Hemming, S.R., Grousset, F.E., 2009. Contrasting compositions of Saharan dust in the eastern Atlantic Ocean during the last deglaciation and African Humid Period. Earth Planet. Sci. Lett. 278, 257–266.

Colin, C., Turpin, L., Blamart, D., Frank, N., Kissel, C., Duchamp, S., 2006. Evolution of weathering patterns in the Indo-Burman Ranges over the last 280 kyr: Effects of sediment provenance on $^{87}Sr/^{86}Sr$ ratios tracer. Geochem. Geophys. Geosyst. 7, Q03007 https://doi.org/10.1029/2005GC000962.

Dasch, E.J., 1969. Strontium isotopes in weathering profiles, deep-sea sediments, and sedimentary rocks. Geochim. Cosmochim. Acta 33, 1521–1552.

De Lange, G.J., Boelrijk, N.A.I.M., Catalano, G., Corselli, C., Klinkhammer, G.P., Middelburg, J.J., Müller, D.W., Ullman, W.J., Van Gaans, P., Woittiez, J.R.W., 1990. Sulphate related equilibria in the hypersaline brines of the Tyro and Bannock basins, eastern Mediterranean. Mar. Chem. 31, 89–112.

De Lange, G.J., Thomson, J., Reitz, A., Slomp, C.P., Principato, M.S., Erba, E., Corselli, C., 2008. Synchronous basin-wide formation and redox-controlled preservation of a Mediterranean sapropel. Nat. Geosci. 1, 606–610.

Dehairs, F., Chesselet, R., Jedwab, J., 1980. Discrete suspended particles of barite and the barium cycle in the open ocean. Earth Planet. Sci. Lett. 49, 528–550.

Dehairs, F., Fagel, N., Antia, A.N., Peinert, R., Elskens, M., Goeyens, L., 2000. Export production in the Bay of Biscay as estimated from barium - barite in settling material: a comparison with new production. Deep-Sea Res. Part I Oceanogr. Res. Papers 47, 583–601.

Deng, N., Stack, A.G., Weber, J., Cao, B., De Yoreo, J.J., Hu, Y., 2019a. Organic–mineral interfacial chemistry drives heterogeneous nucleation of Sr-rich (Ba_x, Sr_{1-x})SO4 from undersaturated solution. Proc. Natl. Acad. Sci. U. S. A. 116, 13221–13226.

Deng, K., Yang, S.Y., Bi, L., Chang, Y.P., Su, N., Frings, P., Xie, X.L., 2019b. Small dynamic mountainous rivers in Taiwan exhibit large sedimentary geochemical and provenance heterogeneity over multi-spatial scales. Earth Planet. Sci. Lett. 505, 96–109.

Dymond, J., Suess, E., Lyle, M., 1992. Barium in deep-sea sediment: a geochemical proxy for paleoproductivity. Paleoceanography 7, 163–181.

Eagle, M., Paytan, A., Arrigo, K.R., van Dijken, G., Murray, R.W., 2003. A comparison between excess barium and barite as indicators of carbon export. Paleoceanography 18, 1021. https://doi.org/10.1029/2002PA000793.

Eisenhauer, A., Meyer, H., Rachold, V., Tutken, T., Wiegand, B., Hansen, B., Spielhagen, R., Lindemann, F., Kassens, H., 1999. Grain size separation and sediment mixing in Arctic Ocean sediments: evidence from the strontium isotope systematic. Chem. Geol. 158, 173–188.

Fagel, N., Andre, L., Dehairs, F., 1999. Advective excess Ba transport as shown from sediment and trap geochemical signatures. Geochim. Cosmochim. Acta 63, 2353–2367.

Fantle, M.S., Barnes, B.D., Lau, K.V., 2020. The role of diagenesis in shaping the geochemistry of the marine carbonate record. Annu. Rev. Earth Planet. Sci. 2020, 549–583.

Feng, J.-L., Zhu, L., Zhen, X., Hu, Z., 2009. Grain size effect on Sr and Nd isotopic compositions in eolian dust: Implications for tracing dust provenance and Nd model age. Geochem. J. 43 (2), 123–131.

Filippidi, A., Triantaphyllou, M.V., de Lange, G.J., 2016. Eastern-Mediterranean ventilation variability during sapropel S1 formation, evaluated at two sites influenced by deep-water formation from Adriatic and Aegean Seas. Quat. Sci. Rev. 144, 95–106.

Francois, R., Honjo, S., Manganini, S.J., Ravizza, G.E., 1995. Biogenic barium fluxes to the deep-sea - Implications for paleoproductivity reconstruction. Glob. Biogeochem. Cycles 9, 289–303.

Freydier, R., Michard, A., de Lange, G.J., Thomson, J., 2001. Nd isotopic compositions of Eastern Mediterranean sediments: tracers of the Nile influence during sapropel S1 formation? Mar. Geol. 177, 45–62.

Ganeshram, R.S., Francois, R., Commeau, J., Brown-Leger, S.L., 2003. An experimental investigation of Barite formation in seawater. Geochim. Cosmochim. Acta 67, 2599–2605.

Gingele, F., Dahmke, A., 1994. Discrete barite particles and barium as tracers of paleoproductivity in South Atlantic sediments. Paleoceanography 9, 151–168.

Gonneea, M.E., Paytan, A., 2006. Phase associations of barium in marine sediments. Mar. Chem. 100, 124–135.

Gonzalez-Munoz, M.T., Martinez-Ruiz, F., Morcillo, F., Martin-Ramos, J.D., Paytan, A., 2012. Precipitation of barite by marine bacteria: a possible mechanism for marine barite formation. Geology 40, 675–678.

Govindaraju, K., 1994. 1994 compilation of working values and sample description for 383 geostandards. Geostand. Geoanal. Res. 18, 1–158.

Griffith, E.M., Paytan, A., 2012. Barite in the ocean – occurrence, geochemistry and palaeoceanographic applications. Sedimentology 59, 1817–1835.
Grousset, F.E., Biscaye, P.E., 2005. Tracing dust sources and transport patterns using Sr, Nd and Pb isotopes. Chem. Geol. 222, 149–167.
Grousset, F.E., Parra, M., Bory, A., Martinez, P., Bertrand, P., Shimmield, G., Ellam, R.M., 1998. Saharan wind regimes traced by the Sr-Nd isotopic composition of subtropical Atlantic sediments: Last Glacial maximum vs. today. Quat. Sci. Rev. 17, 395–409.
Hemming, S.R., van de Flierdt, T., Goldstein, S.L., Franzese, A.M., Roy, M., Gastineau, G., Landrot, G., 2007. Strontium isotope tracing of terrigenous sediment dispersal in the Antarctic Circumpolar Current: Implications for constraining frontal positions. Geochem. Geophys. Geosyst. 8 https://doi.org/10.1029/2006GC001441. Q06N13.
Hennekam, R., Donders, T., Zwiep, K., de Lange, G., 2015. Integral view of Holocene precipitation and vegetation changes in the Nile catchment area as inferred from its delta sediments. Quat. Sci. Rev. 130, 189–199.
House, B.M., Norris, R.D., 2020. Unlocking the barite paleoproductivity proxy: a new high-throughput method for quantifying barite in marine sediments. Chem. Geol. 552, 119664.
Jaccard, S.L., Galbraith, E.D., Sigman, D.M., Haug, G.H., 2010. A pervasive link between Antarctic ice core and subarctic Pacific sediment records over the past 800 kyrs. Quat. Sci. Rev. 29, 206–212.
Jaccard, S.L., Hayes, C.T., Martínez-García, A., Hodell, D.A., Anderson, R.F., Sigman, D. M., Haug, G.H., 2013. Two modes of change in Southern Ocean productivity over the past million years. Science 339, 1419–1423.
Jochum, K.P., Nohl, L., Herwig, K., Lammel, E., Stoll, B., Hofmann, A.W., 2005. GeoReM: a new geochemical database for reference materials and isotopic standards. Geostand. Geoanal. Res. 29, 333–338.
Jung, S.J.A., Davies, G.R., Ganssen, G.M., Kroon, D., 2004. Stepwise Holocene aridification in NE Africa deduced from dust-borne radiogenic isotope records. Earth Planet. Sci. Lett. 221, 27–37.
Kastner, M., 1999. Oceanic minerals: their origin, nature of their environment and significance. Proc. Natl. Acad. Sci. U. S. A. 96, 3380–3387.
Klump, J., Hebbeln, D., Wefer, G., 2000. The impact of sediment provenance on barium-based productivity estimates. Mar. Geol. 169, 259–271.
Krabbenhöft, A., Eisenhauer, A., Böhm, F., Vollstaedt, H., Fietzke, J., Liebetrau, V., Augustin, N., Peucker-Ehrenbrink, B., Müller, M.N., Horn, C., Hansen, B.T., Nolte, N., Wallmann, K., 2010. Constraining the marine strontium budget with natural strontium isotope fractionations ($^{87}Sr/^{86}Sr^*$, $\delta^{88}/^{86}Sr$) of carbonates, hydrothermal solutions and river waters. Geochim. Cosmochim. Acta 74, 4097–4109.
Krom, M.D., Michard, A., Cliff, R.A., Strohle, K., 1999. Sources of sediment to the Ionian Sea and western Levantine basin of the Eastern Mediterranean during S-1 sapropel times. Mar. Geol. 160, 45–61.
Langereis, C.G., Dekkers, M.J., De Lange, G.J., Paterne, M., Van Santvoort, P.J.M., 1997. Magnetostratigraphy and astronomical calibration of the last 1.1 Myr from a Central Mediterranean piston core and dating of short events in the Brunhes. Geophys. J. Int. 129, 75–94.
Lea, D.W., Boyle, E.A., 1989. Barium content of benthic foraminifera controlled by bottom-water composition. Nature 338, 751–753.
Lea, D.W., Boyle, E.A., 1993. Determination of carbonate-bound barium in corals and foraminifera by isotope dilution plasma mass spectrometry. Chem. Geol. 103, 73–84.
Light, T., Norris, R., 2021. Quantitative visual analysis of marine barite microcrystals: Insights into precipitation and dissolution dynamics. Limnol. Oceanogr. 66, 3619–3629.
Liu, Z.F., Colin, C., Huang, W., Le, K.P., Tong, S.Q., Chen, Z., Trentesaux, A., 2007. Climatic and tectonic controls on weathering in South China and Indochina Peninsula: Clay mineralogical and geochemical investigations from the Pearl, Red, and Mekong drainage basins. Geochem. Geophys. Geosyst. 8, Q05005 https://doi.org/10.1029/2006GC001490.
Lyle, M., Heath, G.R., Robbins, J.M., 1984. Transport and release of transition-elements during early diagenesis - sequential leaching of sediments from Manop Site-M and Site-H. part I. pH 5 acetic acid leach. Geochim. Cosmochim. Acta 48, 1705–1715.
Ma, Z., Gray, E., Thomas, E., Murphy, B., Zachos, J., Paytan, A., 2014. Carbon sequestration during the Palaeocene–Eocene thermal Maximum by an efficient biological pump. Nat. Geosci. 7, 382–388.
Martinez-Ruiz, F., Kastner, M., Paytan, A., Ortega-Huertas, M., Bernasconi, S.M., 2000. Geochemical evidence for enhanced productivity during S1 sapropel deposition in the eastern Mediterranean. Paleoceanography 15, 200–209.
Martinez-Ruiz, F., Jroundi, F., Paytan, A., Guerra-Tschuschke, I., Abad, M.D., Gonzalez-Munoz, M.T., 2018. Barium bioaccumulation by bacterial biofilms and implications for Ba cycling and use of Ba proxies. Nat. Commun. 9, 1619. https://doi.org/10.1038/s41467-018-04069-z.
Martinez-Ruiz, F., Paytam, A., Gonzalez-Munoz, M.T., Jroundi, F., Abad, M.M., Lam, P.J., Bishop, J.K.B., Horner, T.J., Morton, P.L., Kastner, M., 2019. Barite formation in the ocean: Origin of amorphous and crystalline precipitates. Chem. Geol. 511, 441–451.
McManus, J., Berelson, W.M., Klinkhammer, G.P., Johnson, K.S., Coale, K.H., Anderson, R.F., Kumar, N., Burdige, D.J., Hammond, D.E., Brumsack, H.J., McCorkle, D.C., Rushdi, A., 1998. Geochemistry of barium in marine sediments: Implications for its use as a paleoproxy. Geochim. Cosmochim. Acta 62, 3453–3473.
Meyer, I., Davies, G.R., Stuut, J.B.W., 2011. Grain size control on Sr-Nd isotope provenance studies and impact on paleoclimate reconstructions: an example from deep-sea sediments offshore NW Africa. Geochem. Geophys. Geosyst. 12, Q03005 https://doi.org/10.1029/2010GC003355.
Monnin, C., Cividini, D., 2006. The saturation state of the world's ocean with respect to $(Ba,Sr)SO_4$ solid solutions. Geochim. Cosmochim. Acta 70, 3290–3298.
Murat, A., Got, H., 2000. Organic carbon variations of the eastern Mediterranean Holocene sapropel: a key for understanding formation processes. Palaeogeogr. Palaeoclimatol. Palaeoecol. 158, 241–257.
Nesbitt, H.W., Markovics, G., Price, R.C., 1980. Chemical processes affecting alkalis and alkaline-earths during continental weathering. Geochim. Cosmochim. Acta 44, 1659–1666.
Passier, H.F., Middelburg, J.J., de Lange, G.J., Bottcher, M.E., 1997. Pyrite contents, microtextures, and sulfur isotopes in relation to formation of the youngest eastern Mediterranean sapropel. Geology 25, 519–522.
Paytan, A., Griffith, E.M., 2007. Marine barite: Recorder of variations in ocean export productivity. Deep-Sea Res. Part II Top. Stud. Oceanogr. 54, 687–705.
Paytan, A., Kastner, M., 1996. Benthic Ba fluxes in the central Equatorial Pacific, implications for the oceanic Ba cycle. Earth Planet. Sci. Lett. 142, 439–450.
Paytan, A., Kastner, M., Martin, E.E., Macdougall, J.D., Herbert, T., 1993. Marine barite as a monitor of seawater strontium isotope composition. Nature 366, 445–449.
Paytan, A., Kastner, M., Chavez, F.P., 1996. Glacial to interglacial fluctuations in productivity in the equatorial Pacific as indicated by marine barite. Science 274, 1355–1357.
Paytan, A., Mearon, S., Cobb, K.M., Kastner, M., 2002. Origin of marine barite deposits: Sr and S isotope characterization. Geology 30, 747–750.
Paytan, A., Griffith, E.M., Eisenhauer, A., Hain, M.P., Wallmann, K., Ridgwell, A., 2021. A 35-million-year record of seawater stable Sr isotopes reveals a fluctuating global carbon cycle. Science 371, 1346–1350.
Pearce, C.R., Parkinson, I.J., Gaillardet, J., Charlier, B.L.A., Mokadem, F., Burton, K.W., 2015. Reassessing the stable ($\delta^{88/86}Sr$) and radiogenic ($^{87}Sr/^{86}Sr$) strontium isotopic composition of marine inputs. Geochim. Cosmochim. Acta 157, 125–146.
Planchon, F., Cavagna, A.-J., Cardinal, D., Andre, L., Dehairs, F., 2013. Late summer particulate organic carbon export and twilight zone remineralisation in the Atlantic sector of the Southern Ocean. Biogeosciences 10, 803–820.
Putnis, C.V., Kowacz, M., Putnis, A., 2008. The mechanism and kinetics of DTPA-promoted dissolution of barite. Appl. Geochem. 23, 2778–2788.
Reitz, A., Pfeifer, K., de Lange, G.J., Klump, J., 2004. Biogenic barium and the detrital Ba/Al ratio: a comparison of their direct and indirect determination. Mar. Geol. 204, 289–300.
Reitz, A., Thomson, J., de Lange, G.J., Hensen, C., 2006a. Source and development of large manganese enrichments above eastern Mediterranean sapropel S1. Paleoceanography 21, PA3007. https://doi.org/10.1029/2005PA001169.
Reitz, A., Thomson, J., de Lange, G.J., Green, D.R.H., Slomp, C.P., Gebhardt, A.C., 2006b. Effects of the Santorini (Thera) eruption on manganese behavior in Holocene sediments of the eastern Mediterranean. Earth Planet. Sci. Lett. 241, 188–201.
Revel, M., Ducassou, E., Grousset, F.E., Bernasconi, S.M., Migeon, S., Revillon, S., Mascle, J., Murat, A., Zaragosi, S., Bosch, D., 2010. 100,000 years of African monsoon variability recorded in sediments of the Nile margin. Quat. Sci. Rev. 29, 1342–1362.
Robin, E., Rabouille, C., Martinez, G., Lefevre, I., Reyss, J.L., van Beek, P., Jeandel, C., 2003. Direct barite determination using SEM/EDS-ACC system: implication for constraining barium carriers and barite preservation in marine sediments. Mar. Chem. 82, 289–306.
Rohling, E.J., Palike, H., 2005. Centennial-scale climate cooling with a sudden cold event around 8,200 years ago. Nature 434, 975–979.
Rohling, E.J., Marino, G., Grant, K.M., 2015. Mediterranean climate and oceanography, and the periodic development of anoxic events (sapropels). Earth Sci. Rev. 143, 62–97.
Rossignol-Strick, M., Nesteroff, W., Olive, P., Vergnaud-Grazzini, C., 1982. After the deluge: Mediterranean stagnation and sapropel formation. Nature 295, 105–110.
Rushdi, A.I., McManus, J., Collier, R.W., 2000. Marine barite and celestite saturation in seawater. Mar. Chem. 69, 19–31.
Rutberg, R.L., Goldstein, S.L., Hemming, S.R., Anderson, R.F., 2005. Sr isotope evidence for sources of terrigenous sediment in the Southeast Atlantic Ocean: is there increased available Fe for enhanced glacial productivity? Paleoceanography 20, PA1018. https://doi.org/10.1029/2003PAO00999.
Rutten, A., de Lange, G.J., 2002. A novel selective extraction of barite, and its application to eastern Mediterranean sediments. Earth Planet. Sci. Lett. 198, 11–24.
Schenau, S.J., Prins, M.A., de Lange, G.J., Monnin, C., 2001. Barium accumulation in the Arabian Sea: Controls on barite preservation in marine sediments. Geochim. Cosmochim. Acta 65, 1545–1556.
Scheuvens, D., Schutz, L., Kandler, K., Ebert, M., Weinbruch, S., 2013. Bulk composition of northern African dust and its source sediments–a compilation. Earth Sci. Rev. 116, 170–194.
Siani, G., Paterne, M., Michel, E., Sulpizio, R., Sbrana, A., Arnold, M., Haddad, G., 2001. Mediterranean Sea surface radiocarbon reservoir age changes since the last glacial maximum. Science 294, 1917–1920.
Slomp, C.P., Thomson, J., de Lange, G.J., 2002. Enhanced regeneration of phosphorus during formation of the most recent eastern Mediterranean sapropel (S1). Geochim. Cosmochim. Acta 66, 1171–1184.
Slomp, C.P., Thomson, J., de Lange, G.J., 2004. Controls on phosphorus regeneration and burial during formation of eastern Mediterranean sapropels. Mar. Geol. 203, 141–159.
Stein, M., Almogi-Labin, A., Goldstein, S.L., Hemleben, C., Starinsky, A., 2007. Late Quaternary changes in desert dust inputs to the Red Sea and Gulf of Aden from Sr-87/Sr-86 ratios in deep-sea cores. Earth Planet. Sci. Lett. 261, 104–119.
Stevenson, R., Pearce, C.R., Rosa, E., Helie, J.F., Hillaire-Marcel, C., 2018. Weathering processes, catchment geology and river management impacts on radiogenic ($^{87}Sr/^{86}Sr$) and stable ($\delta^{88/86}Sr$) strontium isotope compositions of Canadian boreal rivers. Chem. Geol. 486, 50–60.

Tachikawa, K., Roy-Barman, M., Michard, A., Thouron, D., Yeghicheyan, D., Jeandel, C., 2004. Neodymium isotopes in the Mediterranean Sea: Comparison between seawater and sediment signals. Geochim. Cosmochim. Acta 68, 3095–3106.
Thirlwall, M.F., 1991. Long-term reproducibility of multicollector Sr and Nd isotope analysis. Chem. Geol. 94, 85–104.
Thomson, J., Higgs, N.C., Wilson, T.R.S., Croudace, I.W., de Lange, G.J., van Santvoort, P.J.M., 1995. Redistribution and geochemical behavior of redox-sensitive elements around S1, the most recent Eastern Mediterranean sapropel. Geochim. Cosmochim. Acta 59, 3487–3501.
Thomson, J., Mercone, D., de Lange, G.J., van Santvoort, P.J.M., 1999. Review of recent advances in the interpretation of eastern Mediterranean sapropel S1 from geochemical evidence. Mar. Geol. 153, 77–89.
Torres-Crespo, N., Martinez-Ruiz, F., Gonzalez-Munoz, M.T., Bedmar, E.J., de Lange, G. J., Jroundi, F., 2015. Role of bacteria in marine barite precipitation: a case study using Mediterranean seawater. Sci. Total Environ. 512, 562–571.
Tribovillard, N.P., Caulet, J.P., Vergnaud-Grazzini, C., Moureau, N., Tremblay, P., 1996. Lack of organic matter accumulation on the upwelling-influenced Somalia margin in a glacial–interglacial transition. Mar. Geol. 133, 157–182.
van Beek, P., Reyss, J.L., Bonte, P., Schmidt, S., 2003. Sr/Ba in barite: a proxy of barite preservation in marine sediments? Mar. Geol. 199, 205–220.
van Beek, P., Francois, R., Conte, M., Reyss, J.L., Souhaut, M., Charette, M., 2007. ^{22}8Ra/^{226}Ra and ^{226}Ra/Ba ratios to track barite formation and transport in the water column. Geochim. Cosmochim. Acta 71, 71–86.
Van Dijk, D., Houba, V.J.G., 2000. Homogeneity and stability of materials distributed within the Wageningen evaluating programmes for analytical laboratories. Commun. Soil Sci. Plant Anal. 31, 1745–1756.
Van Santvoort, P.J.M., de Lange, G.J., Thomson, J., Cussen, H., Wilson, T.R.S., Krom, M. D., Ströhle, K., 1996. Active post-depositional oxidation of the most recent sapropel (S1) in sediments of the eastern Mediterranean Sea. Geochim. Cosmochim. Acta 60, 4007–4024.
Vance, D., Teagle, D.A.H., Foster, G.L., 2009. Variable Quaternary chemical weathering fluxes and imbalances in marine geochemical budgets. Nature 458, 493–496.
Walter, H.J., Hegner, E., Diekmann, B., Kuhn, G., van der Loeff, M.M.R., 2000. Provenance and transport of terrigenous sediment in the South Atlantic Ocean and their relations to glacial and interglacial cycles: Nd and Sr isotopic evidence. Geochim. Cosmochim. Acta 64, 3813–3827.
Wei, G.J., Ma, J.L., Liu, Y., Xie, L.H., Lu, W.J., Deng, W.F., Ren, Z.Y., Zeng, T., Yang, Y.H., 2013. Seasonal changes in the radiogenic and stable strontium isotopic composition of Xijiang River water: Implications for chemical weathering. Chem. Geol. 343, 67–75.
Weldeab, S., Emeis, K.C., Hemleben, C., Siebel, W., 2002. Provenance of lithogenic surface sediments and pathways of riverine suspended matter in the Eastern Mediterranean Sea: evidence from ^{143}Nd/^{144}Nd and ^{87}Sr/^{86}Sr ratios. Chem. Geol. 186, 139–149.
Widanagamage, I.H., Griffith, E.M., Singer, D.M., Scher, H.D., Buckley, W.P., Senko, J. M., 2015. Controls on stable Sr-isotope fractionation in continental barite. Chem. Geol. 411, 215–227.
Wu, J.W., Böning, P., Pahnke, K., Tachikawa, K., de Lange, G.J., 2016. Unraveling North-African riverine and eolian contributions to Central Mediterranean sediments during Holocene sapropel S1 formation. Quat. Sci. Rev. 152, 31–48.
Wu, J.W., Liu, Z., Stuut, J.-B.W., Zhao, Y., Schirone, A., de Lange, G.J., 2017. North-African paleodrainage discharges to the Central Mediterranean during the last 18,000 years: a multiproxy characterization. Quat. Sci. Rev. 163, 95–113.
Wu, J.W., Filippidi, A., Davies, G.R., de Lange, G.J., 2018. Riverine supply to the eastern Mediterranean during last interglacial sapropel S5 formation: a basin-wide perspective. Chem. Geol. 485, 74–89.
Wu, J.W., Pahnke, K., Böning, P., Wu, L., Michard, A., de Lange, G.J., 2019. Divergent Mediterranean seawater circulation during Holocene sapropel formation – Reconstructed using Nd isotopes in fish debris and foraminifera. Earth Planet. Sci. Lett. 511, 141–153.
Xie, R.C., Marcantonio, F., 2012. Deglacial dust provenance changes in the Eastern Equatorial Pacific and implications for ITCZ movement. Earth Planet. Sci. Lett. 317–318, 386–395.
Zhao, Y.L., Colin, C., Liu, Z.F., Paterne, M., Siani, G., Xie, X., 2012. Reconstructing precipitation changes in northeastern Africa during the Quaternary by clay mineralogical and geochemical investigations of Nile deep-sea fan sediments. Quat. Sci. Rev. 57, 58–70.
Ziegler, C.L., Murray, R.W., Hovan, S.A., Rea, D.K., 2007. Resolving eolian, volcanogenic, and authigenic components in pelagic sediment from the Pacific Ocean. Earth Planet. Sci. Lett. 254, 416–432.